Influence of dynamic elements in stable tissue phantoms on laser speckle decorrelation times

Bachelor Thesis Technische Natuurkunde

Names:	*Martin Buitink*
	Rieks Hekman
Supervisor:	*Dr. ir. I.M. Vellekoop*
	Biomedical Photonic Imaging

--- 23 - 04- 2014 ---

Faculteit Technische Natuurwetenschappen

Universiteit Twente

2014

Summary

In this report the decorrelation of a speckle pattern created by the transmission of laser light through a stable tissue phantom with a scattering fluid flowing through a tube inside is discussed.

After the introduction, theory is developed and adapted from literature in chapter 2 to describe this process. This is done along three lines.

First, in section 2.1, an equation based on one-dimensional diffusion theory to calculate the amount of transmitted light that went through the tube in the sample is derived and discussed. As is shown in section 2.2, with this equation, the normalized autocorrelation function of the speckle pattern can be expressed in terms of the geometrical parameters of the sample and the intermediate scattering function as follows:

$$g_{\beta}^{(2)}(\tau) = 1 + \beta\left(\left(1 - \frac{2r_t}{\pi r}\right)^2 + 2\left(1 - \frac{2r_t}{r}\right)\frac{2r_t}{r}|G(\tau)| + \left(\frac{2r_t}{r}\right)^2 |G(\tau)|^2\right),$$

where r_t is the radius of the tube, r is the radius of the illuminated area, β is an instrumental factor ranging between 0 and 1 and $G(\tau)$ is the intermediate scattering function. Two existing models are adapted in section 2.3 to find an expression for the intermediate scattering function $G(\tau)$. One is generally used in Laser Doppler Flowmetry (LDF) and includes both Brownian and translational movement. The other is based on Diffusing Wave Spectroscopy (DWS) and incorporates only Brownian motion. These models, which result in very distinctive autocorrelation functions, are compared and discussed in this same section.

As a third and more basic theoretical approach, laminar flow of a fluid in a tube was considered in section 2.4. An equation was derived for the time scale of decorrelation effects caused by translation of the fluid:

$$t_{95} = \frac{\lambda \pi r_t^2}{0.2\, Q},$$

where λ is the wavelength of the light used and Q is the discharge. Though this equation gives no predictions about the shape or half times of the autocorrelation function, it gives an upper limit of the time scales on which decorrelation caused by *translational* motion of the fluid can take place. A final conclusion and discussion of the theoretical chapter 2 is given in section 2.5.

Chapter 3 covers the experimental aspects of this research. In section 3.1, the predictions coming from the different models are discussed. Apart from the fact that the shapes of the autocorrelation functions from the LDF and DWS model differ, the time scales also differ a lot: for a 2.2 mm diameter tube, half times are in the range of 10^{-8} s for the LDF model, and in the range of 10^{-5} s for the DWS model. Meanwhile, the tube flow considerations give an upper limit to the time scales of decorrelation caused by fluid motion in the range of 10^{-4} s for the discharges considered in this report (excluding Q = 0).

Section 3.2 explains the setup used in the experiments and gives relevant specifications (material parameters, camera specifications etc.). The experimental results are shown and discussed in the following section, 3.3. The experiments were done on two Delrin slabs, one with a 2.2 mm and the

other with a 3.2 mm diameter tube. Intralipid 10% was used as a scattering fluid. It appears that, while Brownian motion gives visible effects in the range of 10^{-3} s, the translational motion is so fast in the 2.2 mm tube experiments that it gives effects on time scales within the camera shutter time, making the results hard to interpret. For the larger tube, in which fluid velocity is lower, indeed decorrelation times decrease with increasing fluid velocity.

Still, the experiments do not agree with theory. Most notably, for Q = 0, the effects of Brownian motion are seen on a much slower basis than predicted by the LDF as well as the DWS model. Though the LDF model is in principle capable of predicting decorrelation for nonzero discharges, it gives decorrelation times in the order of 10-8 s, much too fast for our camera to measure. So whether this model gives sensible results for translational motion remains to be seen. Section 3.4 gives a final discussion on the experimental chapter 3 of this report.

In chapter 4, the conclusions from the various parts of this research are summarized. Finally, the used references are given at the end of this report.

Contents

1. Introduction

When light travels through an optically turbid medium, it becomes multiply scattered. The transmitted light will create a disordered interference pattern called speckle. For monochromatic light (e.g. from a laser source), this will show up as a pattern of high and low intensity spots with different phases.

Recently, the technique of optical wavefront shaping has been under great interest. In this technique, the shape of wavefronts of light is modified, which makes it possible to focus light behind or even inside highly optically scattering media. While there are different approaches to this technique, most make use of a Spatial Light Modulator to phase shift thousands of incident light modes, creating the shaped wavefront. This can be done iteratively – phase shifting the modes one by one until maximum intensity is reached at the desired location – but this is a relatively time consuming process since extensive feedback is involved. A much faster approach is to measure the speckle caused by a light source and phase conjugate the pattern to refocus at the source location. It is often not possible or desirable to insert a light source inside a medium, but it has been shown that a virtual light source can be created by using ultrasound, which can be focused at any desired place inside the medium. The ultrasound focus is then the location where the phase conjugated light can be focused also.

One of the promising features of this last approach to wavefront shaping is the possibility to focus light inside human tissue. This can be of great use for medical imaging – for instance by scanning the focus through the tissue, activating fluorescent markers at tumor sites – and also for destroying malignant cells without any use of radioactive (carcinogen) radiation and with minimal damage to surrounding cells.

However, focusing light in tissue brings serious challenges, since tissue is not a stable medium. Perfusion and intracellular movements cause the so-called transmission matrix of tissue, which describes how light is scattered inside the medium, to change in time. This raises two important questions: to what extend is this transmission matrix influenced by the dynamic elements in the tissue, and on what time scale do significant changes of this matrix (enough to seriously disturb the phase conjugation process) take place?

In this report, a model is described to investigate the amount of light passing through a dynamic element (a tube with 'blood' flowing inside) in a stable tissue phantom (a slab of Delrin). Three routes are described to predict the decorrelation of the speckle pattern caused by irradiating such a phantom with a laser. These are followed by a discussion of these models and possible improvements. Predictions from the different models are shown and discussed, after which experimental results from actual measurements are shown and compared to the theory. A discussion of the experiments and the discrepancies with the theory follows, to end with our conclusions and recommendations for future research.

2. Theoretical model

The samples used in this research are made of a material that can be considered stable (i.e. the optical transmission matrix does not significantly change in the time scales under investigation). Inside such a sample there is a tube with an optically scattering fluid flowing through. The goal of this section is to show how one can calculate the normalized temporal intensity autocorrelation function, $g^{(2)}(\tau)$ of light passing through a slab with a tube inside, starting from a simple model for one dimensional diffusion of light in a slab. To do this, the following steps are taken:

1. Calculate the ratio between the amount of light that passed specifically through the tube and the total amount of transmitted light by the following steps:
   a. Calculate the energy density and flux resulting from an incoming plane wave at any place inside the slab, and the total power transmitted through the slab to the detector;
   b. Consider a cylindrical tube inside the slab and calculate the power of light going into this tube;
   c. Approximate the tube as a new point source inside the medium that radiates this power, and calculate the amount of light that is transmitted from this source to the detector;
   d. Calculate the ratio between the amount of light that passed specifically through the tube (found in step 1c) and the total amount of transmitted light (found in step 1a);
2. Use this ratio to calculate $g^{(2)}(\tau)$ in terms of the intermediate scattering function $G(\tau)$;
3. Find an expression for $G(\tau)$ using two different approaches from literature.

2.1 Fraction of light going through a tube inside a slab

2.1.1 Equations governing diffusion

Two equations can be used to study diffusion inside a material. The first one is Fick's first law, which states – applied to diffusion of light – that the flux of light (power per unit area) equals some constant times the gradient of the energy density (energy per unit volume):

$$F = -D\nabla u. \tag{1}$$

The constant D is called the diffusion constant and is related to absorption, to the speed of light c and to the mean free path length l of light inside the medium, which is – loosely speaking – the mean distance between two scattering events. In our model we will neglect absorption, in which case

$$D = \frac{lc}{3}. \tag{2}$$

The second equation is an application of the conservation of energy:

$$\frac{\partial u}{\partial t} = -\nabla \cdot F + S - \mu_a c u, \tag{3}$$

where S describes any present light sources and the last term is an absorption term, which scales linearly with the energy density. The proportionality of this scaling is $\mu_a c$, where μ_a is a material constant called the absorption coefficient. Again, in our model we will neglect this term.

2.1.2 One dimensional diffusion in an infinite slab

Consider the situation as depicted schematically in Fig. 1. An infinitely large plane wave enters a slab of thickness L, which extends to infinity in the directions perpendicular to the z-axis.

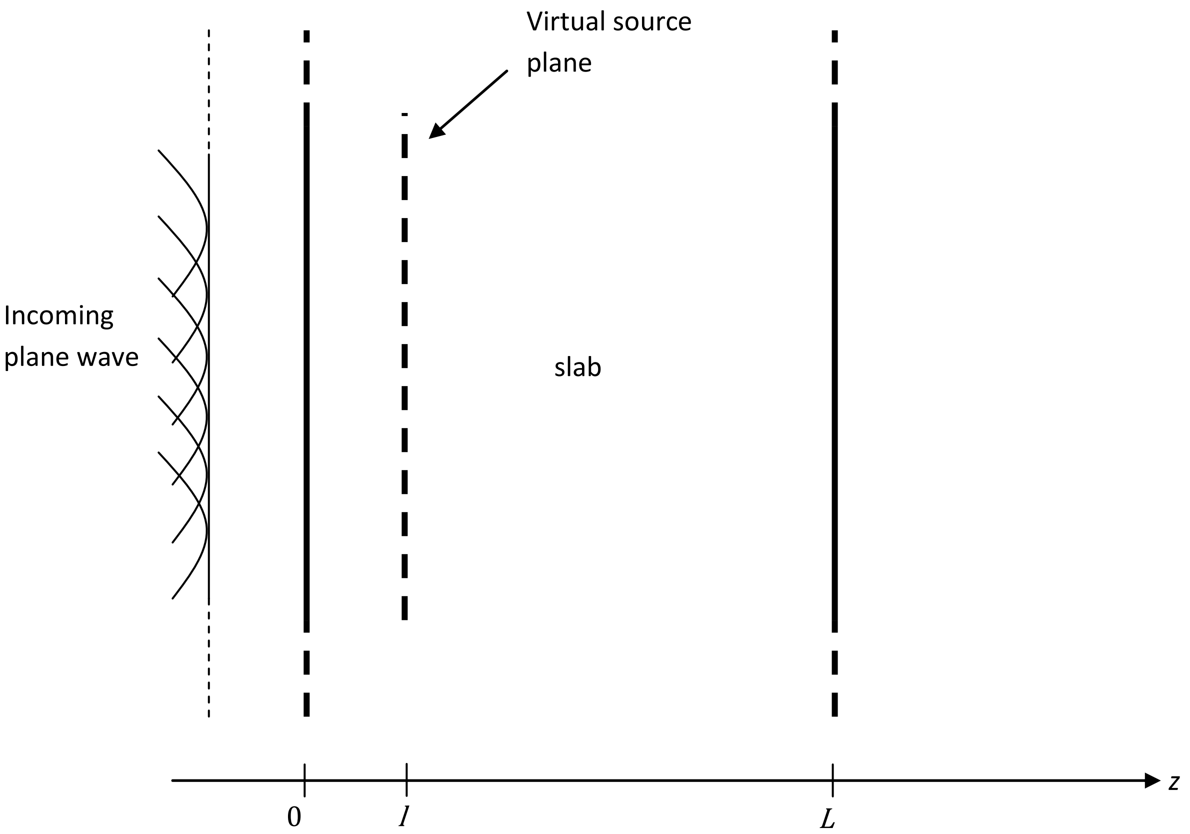

Figure 1. A plane wave entering a slab of thickness L with a virtual source at z = l

This situation can be described by one-dimensional diffusion. It is shown (amongst others) by De Boer[1] that it can be accurately modeled by placing a virtual source S at a distance $z = l$ inside the medium, where l is the mean free path length encountered before. For clarity and also generality, the calculations below will be done for a source at arbitrary location z_0, where in this specific case $z_0 = l$. So, the source term in the diffusion equation now becomes $S = c_1\delta(z - z_0)$, with c_1 a constant. The one dimensional versions of Eq. 1 and Eq. 3 are now:

$$F_z = -D\partial_z u \tag{4}$$

$$\partial_z F_z = c_1\delta(z - z_0), \tag{5}$$

where the time derivative in the diffusion equation has been set equal to zero, because only continuous illumination will be considered. From these equations the second spatial derivative of the energy density can be found:

$$\left.\begin{aligned}\partial_z F_z &= c_1\delta(z - z_0)\\ F_z &= -D\partial_z u\end{aligned}\right\} \Rightarrow \partial_{zz} u = -\frac{c_1}{D}\delta(z - z_0). \tag{6}$$

Integrating this equation gives:

$$\partial_z u = -\frac{c_1}{D}\mathcal{H}(z - z_0) + c_2, \tag{7}$$

with *H* the Heaviside step function. Now, the flux follows from Eq. 4:

$$F = c_1\mathcal{H}(z - z_0) - c_2 D, \tag{8}$$

where from now on the subscript *z* on *F* will be dropped. Integrating Eq. 7 again gives:

$$u = \left(-\frac{c_1}{D}\mathcal{H}(z - z_0)\right)(z - z_0) + c_2 z + c_3, \tag{9}$$

which can also be written as:

$$u = \begin{cases} c_2 z + c_3 & (z < l) \\ \left(-\frac{c_1}{D} + c_2\right) z + \frac{c_1 z_0}{D} + c_3 & (z > l) \end{cases}. \tag{10}$$

Boundary conditions

To find the constants c_1, c_2 and c_3, boundary conditions must be applied. The first two boundary conditions come from the fact that at the boundaries of the slab (z = 0 and z = L) there should be no diffuse intensity entering the medium from outside. De Boer[1] showed that this can be translated into a mixed boundary condition on the average intensity at the boundaries, and this can in turn be translated in a Dirichlet condition which states that the energy density should be zero at an extrapolated distance $z_e = \frac{2}{3}l$ from the boundaries:

$$u(-z_e) = u(L + z_e) = 0. \tag{11}$$

From these two boundary conditions, two of the three constants can be expressed in terms of the remaining one:

$$u(-z_e) = 0 \quad \Rightarrow c_3 = c_2 z_e \tag{12}$$

$$u(L + z_e) = 0 \Rightarrow c_2 = \frac{L + z_e - z_0}{L + 2z_e}\frac{c_1}{D}, \tag{13}$$

The remaining needed boundary condition applies to the flux F. Inserting the expression for c_2 found above in Eq. 8 gives:

$$F = c_1\left(\mathcal{H}(z - z_0) - \frac{L + z_e - z_0}{L + 2z_e}\right). \tag{14}$$

The last constant c_1 can therefore be written as

$$c_1 = F(z > z_0) - F(z < z_0) = |F(z > z_0)| + |F(z < z_0)|, \tag{15}$$

which is just the net total flux coming from the virtual source. To find a physically meaningful value, a finite area with finite incoming power must be considered (in the actual experiment, this will be the illumated area). To match the experimental setup, in this case a circular disc with radius *r* and area $A = \pi r^2$ will be used (see Fig. 2).

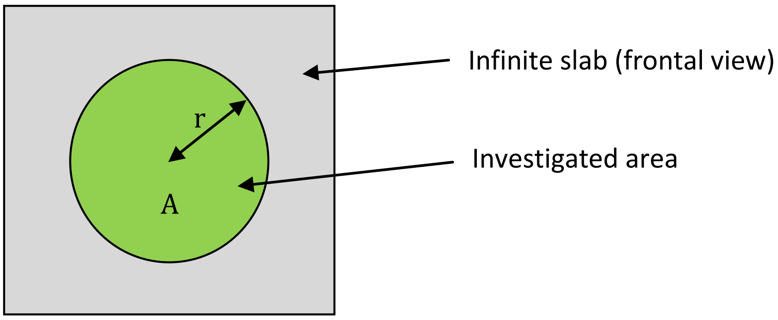

Figure 2. Infinite slab (frontal view, grey) with investigated area A (green)

Now the total flux from the virtual source, c_1, must equal the incoming power divided by the area of incidence:

$$c_1 = \frac{P_{in}}{A}. \tag{16}$$

Now all three constants can be expressed in terms of the incoming power and investigated area. Plugging these expressions into Eq. 8 and Eq. 10 gives for the energy density:

$$u = \begin{cases} \frac{P_{in}}{DA}\left(\frac{L+z_e-z_0}{L+2z_e}\right)(z_e+z) & (z<l) \\ \frac{P_{in}}{DA}\left(\frac{z_e+z_0}{L+2z_e}\right)(L+z_e-z) & (z>l) \end{cases}. \tag{17}$$

and for the flux:

$$F_z = \begin{cases} -\frac{P_{in}}{A}\left(\frac{L+z_e-z_0}{L+2z_e}\right) \equiv -F_{in}R & (z<l) \\ \frac{P_{in}}{A}\left(\frac{z_e+z_0}{L+2z_e}\right) \equiv F_{in}T & (z>l) \end{cases}, \tag{18}$$

where $F_{in} = \frac{P_{in}}{A}$ and R and T are the reflection and transmission coefficients, respectively. These are the solutions for the energy density and flux originating from a source at arbitrary depth z_0 inside a slab of thickness L. They are plotted in Fig. 3. It can easily be seen from Eq. 18 that T+R = 1, as of course should be the case.

Since this all holds for one dimensional diffusion, other dimensions than *z* should remain the same throughout calculations. Therefore, the total transmitted power from a virtual source at depth *z* = *l* can be computed by multiplying the total transmitted flux with an area with size *A*:

$$P_{trans} = AF_{in}T(z_0 = l) = P_{in}\left(\frac{z_e+l}{L+2z_e}\right). \tag{19}$$

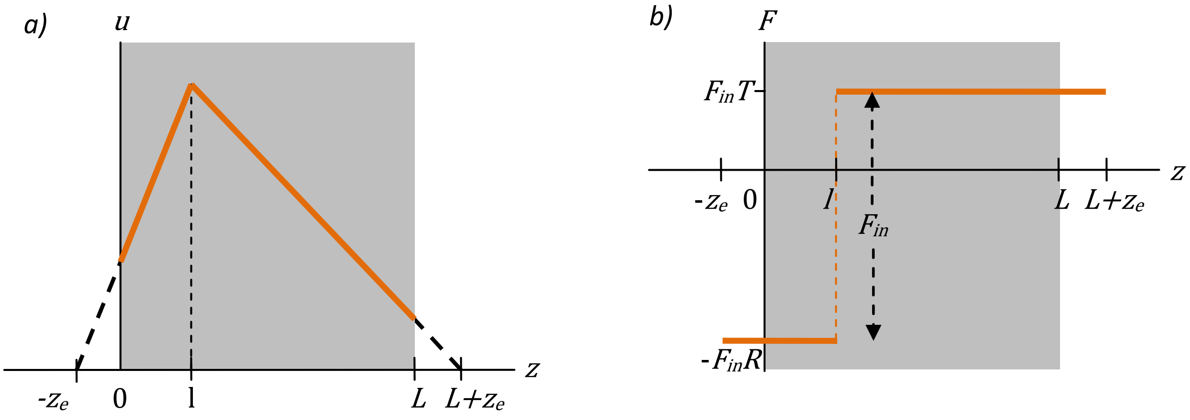

Figure 3. a) Energy density and b) flux distribution for the given slab geometry. Region inside the slab is shaded.

2.1.3 Power entering a tube

Consider the setup of Fig. 4. It is reminiscent of Fig. 1, but a cylindrical tube has been placed at depth $z = z_t$ inside the medium, at the height of the middle of the illuminated area.

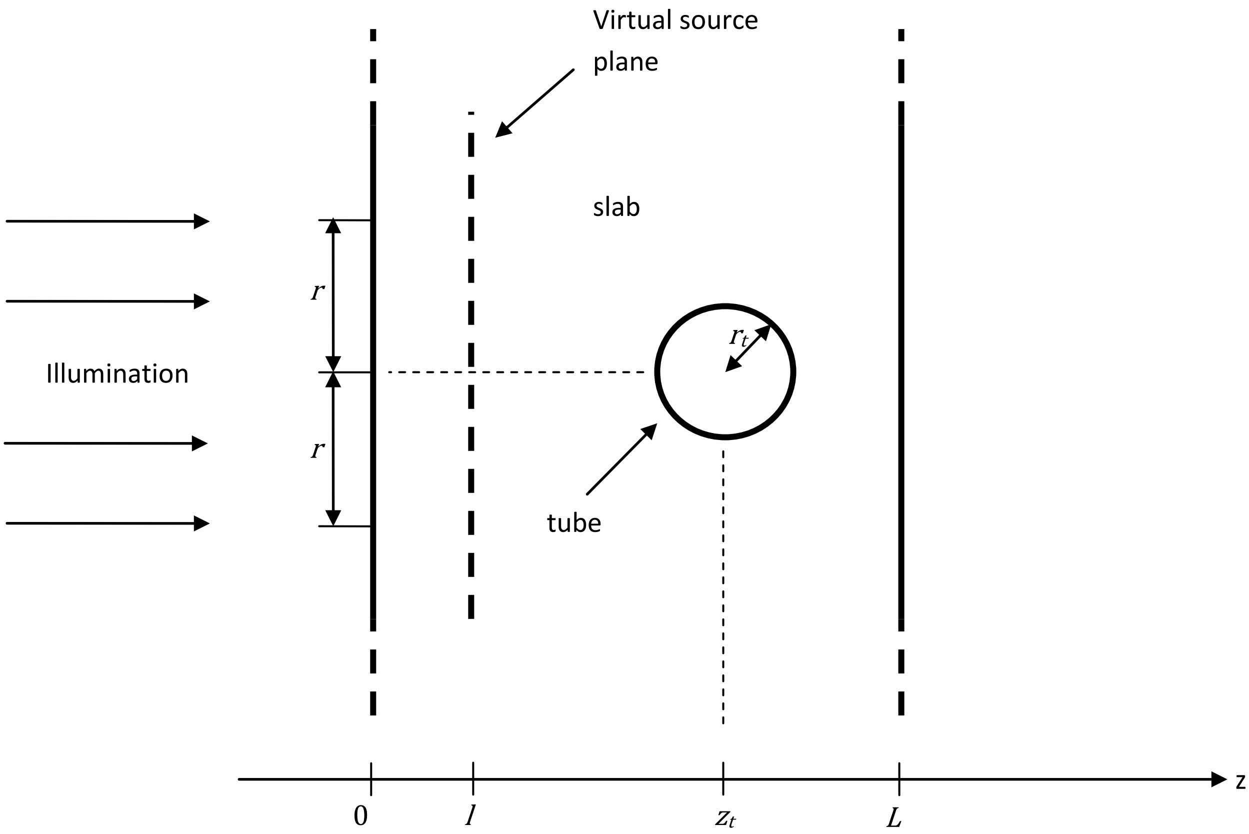

Figure 4. Slab of thickness L with a virtual source at z = l. A cylindrical, infinitely long tube is placed at $z = z_t$, perpendicular to the illumination. A circular area with radius r is illuminated; the center of the tube is at the same height as the center of the illuminated area.

To find the power of diffuse light entering the tube, the following steps are taken:

a. Find the radiance $L(\hat{s})$ from direction $\hat{s}$ (power per unit area per unit of solid angle) at an arbitrary location on the tube surface;
b. Integrate the radiance over a hemisphere of solid angle to find the intensity *I*(*z*): the amount of light going from one side through a unit area patch (power per unit area);
c. Integrate the intensity over the surface area of the tube to find the total incoming power.

In the end, what is needed turns out to be the power of light entering the tube for the first time, without having been there before. To calculate this power from the total power entering the tube involves the probability p_r of light returning to the tube after leaving it. How to calculate this probability still needs to be investigated; instead, an approximation will be used which will make part of the theory developed in this subsection superfluous. Nonetheless, from a theoretical point of view it is interesting to see the steps that could eventually lead to a more precise solution of the problem.

The radiance $L(\vec{s})$ through area dA from direction $\hat{s}$ can be calculated to good approximation by:

$$\begin{aligned} L(\hat{s}) &= \frac{c}{4\pi}u + \frac{3}{4\pi}\vec{F}\cdot\hat{s} \\ &= \frac{c}{4\pi}u(z) + \frac{3}{4\pi}F\hat{z}\cdot\hat{s}, \end{aligned} \tag{20}$$

which will be evaluated in a moment. The intensity can then be found by integrating as follows:

$$I(z) = \int_{2\pi} L(\hat{s})\, \hat{s}\cdot\hat{n}\, d\Omega', \tag{21}$$

where $\hat{n}$ is the normal vector of the chosen unit area patch and $\hat{s}$, as mentioned, is the direction vector, which is swept through a hemisphere of solid angle by the integration, from an angle of $-\frac{\pi}{2}$ to $\frac{\pi}{2}$ radians with $\hat{n}$ (why the notation Ω' is used will be clear in a moment). In Fig. 5 the space through which $\hat{s}$ is swept is indicated by the half circle for a given point at the tube surface.

Because the flux is constant (Eq. 18) in both direction and magnitude for all points on this surface, and the surface is cylindrical (and thus symmetrical) with its axis perpendicular to the z-axis, the nett contribution of the $\vec{F}\cdot\vec{s}$ term to the incoming power is expected to give zero in the end (the positive contribution on the left half of the tube will be balanced by the negative one on the right). But even if this symmetry were not present, the flux term could be left out: if the two terms in $L(\vec{s})$ are compared, it can be seen that the contribution of the flux term is negligible:

$$\frac{3|\vec{F}|}{cu} = \frac{3D}{c(L+z_e-z)} = \frac{l}{(L+z_e-z)}, \tag{22}$$

and this quantity is much smaller than 1 when z is any reasonable distance away from the right side of the slab (such that $L - z \gg l$, while l is typically in the order of a few hundred µm). For completeness, though, the $\vec{F}\cdot\vec{s}$ will be taken along in the calculation.

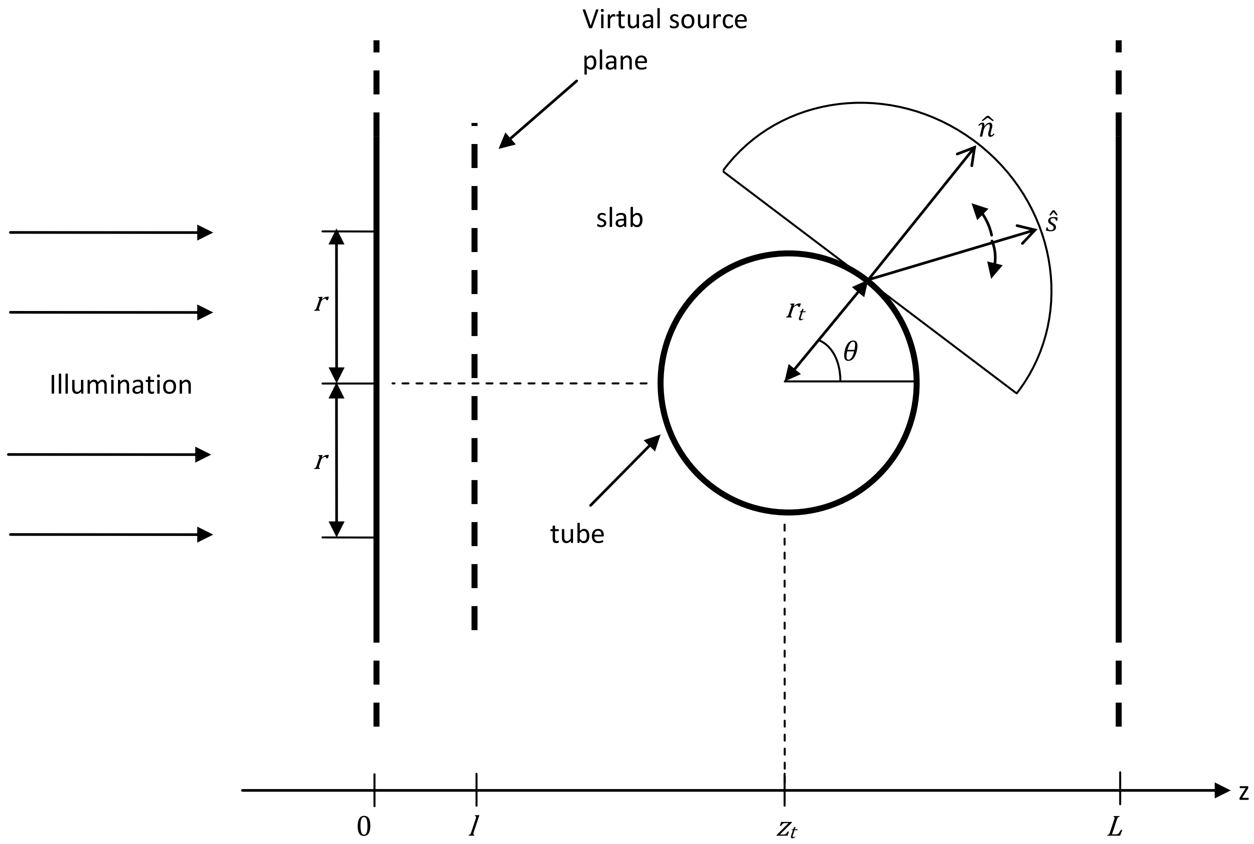

Figure 5. Slab with tube at z_t where the normal and direction vectors $\hat{n}$ and $\hat{s}$ are indicated for a given point on the tube; $\hat{s}$ is swept through a hemisphere of which the vertical cross section is indicated by the half circle.

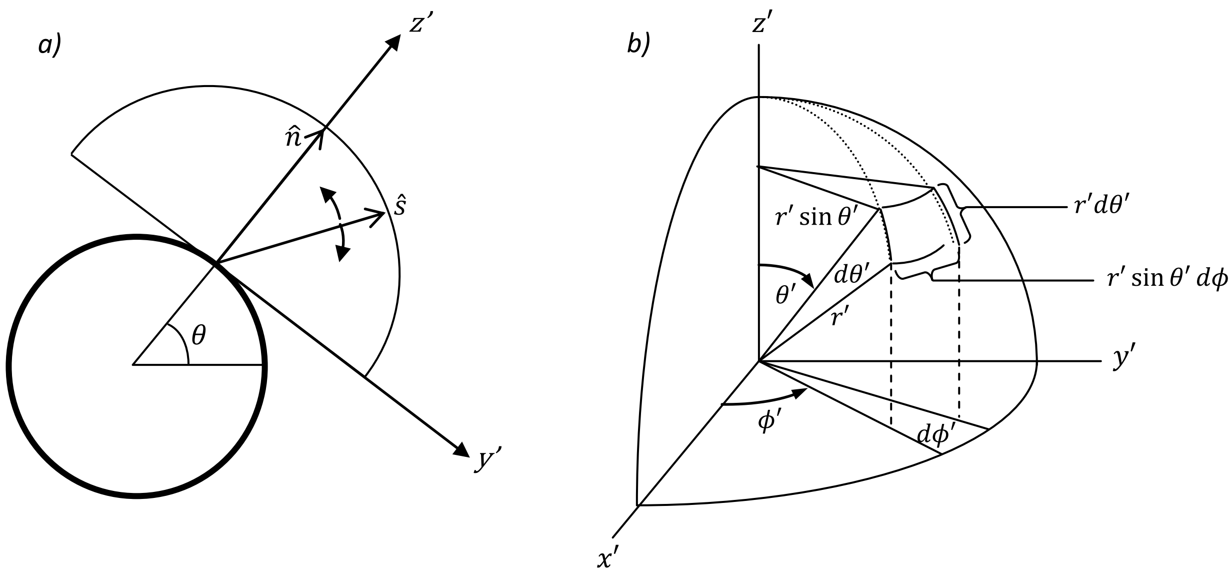

Figure 6. a) Axes y' and z' for a given tube location (x' is directed out of the page); b) indication of the spherical coordinates (r', ϕ', θ') in this system; for the unit vectors used, $r' = 1$.

To further evaluate the expression for $L(\vec{s})$ (and $I(z)$), set up a Cartesian coordinate system (x',y',z') with its base at the point at the tube surface for which $L(\vec{s})$ will be calculated, such that $\hat{n}$ lies along z', x' is directed out of the page toward the reader and y' points in the direction indicated by the right-hand rule (to the right and below in case of Fig. 5 above). It is in this system, shown for a given tube surface location in Fig. 6a , that $I(z)$ will be evaluated, hence also the Ω' notation in Eq. 21.

Defining θ' as the polar angle from z' and ϕ' as the azimuthal angle from x' (see Fig. 6b), the relevant vectors can be expressed as

$$\hat{s} = \sin\theta' \cos\phi' \,\widehat{x'} + \sin\theta' \sin\phi' \,\widehat{y'} + \cos\theta' \,\widehat{z'} \tag{23}$$

$$\hat{n} = \widehat{z'} \tag{24}$$

$$\hat{z} = \sin\theta \,\widehat{y'} + \cos\theta \,\widehat{z'}. \tag{25}$$

For the radiance through a unit area patch at the tube surface this gives:

$$\begin{aligned} L(\hat{s}) &= \frac{c}{4\pi} u(z) + \frac{3}{4\pi} F \hat{z} \cdot \hat{s} \\ &= \frac{c}{4\pi} u(z) + \frac{3}{4\pi} F(\sin\theta \sin\theta' \sin\phi' + \cos\theta \cos\theta'), \end{aligned} \tag{26}$$

and for the intensity:

$$\begin{aligned} I(z) &= \int\limits_{2\pi} L(\hat{s})\, \hat{s} \cdot \hat{n}\, d\Omega' = \int\limits_{2\pi} L(\hat{s}) \cos\theta'\, d\Omega' \\ &= \int\limits_0^{2\pi} \int\limits_0^{\pi/2} L(\hat{s})\, \cos\theta' \sin\theta'\, d\theta'\, d\phi', \end{aligned} \tag{27}$$

where the cosine comes from the $\hat{s} \cdot \hat{n}$ dot product (or, physically, from the fact that the effective area by which the power radiated from angle ϑ is collected is reduced by a factor $\cos\theta$) and the sine from the integration variables: $d\Omega' = \sin\theta'\, d\theta' d\phi'$. Inserting Eq. 26 in Eq. 27 gives:

$$\begin{aligned} I(z) &= \int\limits_0^{2\pi} \int\limits_0^{\pi/2} \left[\frac{c}{4\pi} u(z) + \frac{3}{4\pi} F(\sin\theta \sin\theta' \sin\phi' + \cos\theta \cos\theta')\right] \cos\theta' \sin\theta'\, d\theta'\, d\phi' \\ &= \frac{c}{4\pi} u(z) \int\limits_0^{2\pi} \int\limits_0^{\pi/2} \cos\theta' \sin\theta'\, d\theta'\, d\phi' \\ &\quad + \frac{3}{4\pi} F \left[\sin\theta \int\limits_0^{2\pi} \int\limits_0^{\pi/2} \cos\theta' \sin^2\theta' \sin\phi'\, d\theta'\, d\phi' + \cos\theta \int\limits_0^{2\pi} \int\limits_0^{\pi/2} \cos^2\theta' \sin\theta'\, d\theta'\, d\phi'\right]. \end{aligned}$$

The first term between square brackets is zero, since it involves integrating $\sin\phi'$ from 0 to 2π. Both the other integrals over ϕ' just give 2π, since no ϕ' is involved in the integrand. This gives:

$$
\begin{aligned}
I(z) &= \frac{c}{2}u(z)\int_0^{\pi/2} \cos\theta' \sin\theta'\, d\theta' + \frac{3\cos\theta}{2}F\int_0^{\pi/2} \cos^2\theta' \sin\theta'\, d\theta' \\
&= \frac{c}{2}u(z)\left[\tfrac{1}{2}\sin^2\theta'\right]_0^{\pi/2} + \frac{3\cos\theta}{2}F\left[-\tfrac{1}{3}\cos^3\theta'\right]_0^{\pi/2} \\
&= \frac{c}{4}u(z) + \frac{\cos\theta}{2}F. \qquad (28)
\end{aligned}
$$

This is still generally applicable for any surface to the right of the virtual source with angle θ with z; for the tube surface it holds that $\cos\theta = \frac{z-z_t}{r_t}$ (see Fig. 5), giving:

$$
I(z) = \frac{c}{4}u(z) + \frac{z-z_t}{2r_t}F. \qquad (29)
$$

This equation gives the amount of light entering the tube at a specific location (specified by its z-coordinate).

The power going into the tube can then be computed by:

$$
P_{tube} = \int_{tube} I(z)dA, \qquad (30)
$$

where the integral is carried out over the tube surface. Since both terms in I are linear in z and the tube is symmetrical about $z = z_t$, we can just use the value of $I(z)$ for the middle of the tube, $I(z_t)$, so:

$$
\begin{aligned}
P_{tube} &= \int_{tube} I(z_t)dA = I(z_t)\int_{tube} dA = \left(\frac{c}{4}u(z_t) + 0F\right)(2\pi r_t\, 2r) \\
&= \frac{c\pi r_t r P_{in}}{DA}\left(\frac{z_e + l}{L + 2z_e}\right)(L + z_e - z_t). \qquad (31)
\end{aligned}
$$

This is the expression for the total power going into the tube. Indeed, reassuringly, the flux term becomes zero, as anticipated.

2.1.4 Power entering a tube for the first time

Light that enters the tube is bound to leave it some time. However, after leaving it, it has a certain chance of being scattered in such a way that it enters the tube again. In our model, where we only distinguish between light being dynamically scattered (no matter how much) or not, it is more interesting to know how much light entered the tube *for the first time*. If we call this amount P_1 and the probability of light returning to the tube p_r, the relation between P_1 and the total power P_{tube} entering the tube is given by

$$
P_{tube} = P_1(1 + p_r + p_r^2 + p_r^3 + \cdots) = P_1\sum_{n=0}^{\infty} p_r^n = \frac{P_1}{1-p_r}, \qquad (32)
$$

where the successive terms account for light entering one, two, three, … times. In other words:

$$P_1 = (1 - p_r)P_{tube}, \tag{33}$$

the amount of light entering for the first time is the total amount of light entering times the chance that it does *not* return to the tube (which is $1 - p_r$). If one could calculate the return probability p_r, P_1 could be determined. The tube could then be approximated as a new point source radiating with power P_1 and the transmitted flux of this source can be computed the same way as for the virtual source before.

Determining p_r is beyond the scope of this report. Instead, an approximation will be used. It is assumed that the total amount of light entering the tube for the first time is given by the component of the flux perpendicular to the tube surface, for the left half of the tube. Integrating this over the (left half) tube surface gives:

$$P_1 = \int_{\substack{left\,half \\ of\,tube}} (-\vec{F} \cdot \hat{n})dA \approx -2rF \int_{\pi/2}^{3\pi/2} \cos\theta \, r_t d\theta = 4r_t rF, \tag{34}$$

where it is assumed that $r_t \ll r$, which is just the frontal area of the tube (in the given limit) times F.

2.1.5 Transmitted power from dynamically scattered light

To find the amount of dynamically scattered light that is transmitted to the back of the sample, approximate the tube as a new point source at z_t inside the medium, radiating with power P_1. The transmitted flux of such a point source is given by:

$$F_{trans,tube} = \frac{P_1}{A}\left(\frac{z_e + z_t}{L + 2z_e}\right), \tag{35}$$

in analogy with the virtual source treated before (Eq. 18). Inserting the equation found for P_1 gives for the transmitted flux:

$$F_{trans,tube} = \frac{4r_t rF}{A}\left(\frac{z_e + z_t}{L + 2z_e}\right) = \frac{4r_t rP_{in}}{A^2}\left(\frac{z_e + l}{L + 2z_e}\right)\left(\frac{z_e + z_t}{L + 2z_e}\right), \tag{36}$$

and for the transmitted power:

$$\begin{aligned} P_{trans,tube} &= AF_{trans,tube} = \frac{4r_t rP_{in}}{A}\left(\frac{z_e + l}{L + 2z_e}\right)\left(\frac{z_e + z_t}{L + 2z_e}\right) \\ &= \frac{4r_t P_{in}}{\pi r}\left(\frac{z_e + l}{L + 2z_e}\right)\left(\frac{z_e + z_t}{L + 2z_e}\right). \end{aligned} \tag{37}$$

This is the total power from light entering the tube for the first time that is transmitted to the back of the sample, or in other words, the total detected amount of power from dynamically scattered light.

The overall amount of total transmitted power (of both the dynamical and statical part of the light) is

$$P_{trans} = AF = P_{in}\left(\frac{z_e + z_0}{L + 2z_e}\right). \tag{38}$$

So the fraction of the power of modulated transmitted light to the total power of transmitted light is given by

$$\frac{P_{trans,tube}}{P_{trans}} = \frac{4r_t}{\pi r}\left(\frac{z_e + z_t}{L + 2z_e}\right). \qquad (39)$$

If the total transmitted power would be measured, this equation gives the fraction of it that arises from light that was dynamically scattered because it went through the tube.

2.1.6 Model discussion

It is interesting to see that the fraction of detected power that went through the tube depends linearly on the tube location, increasing as the tube is placed further towards the back of the sample. This dependence originates from Eq. 35, or physically, from the fact that more of the light that leaves the tube will leave the sample at the back when the tube is closer to the back. Considered from the detection point of view, more of the light that is detected will have been through the tube if it is closer to the detection. This is actually a rather strange consequence of Eq. 39, since one would expect by the symmetry of the problem that the fraction of transmitted power (light that went all the way from front to back) that actually went through the tube should be symmetrical around $z_t = L/2$. This indicates that Eq. 39 cannot be more than a first order approximation.

Apart from this transmittance factor between brackets, there is also a factor $4/\pi$ in front. To see where this comes from, forget about the factor between brackets for a moment and consider the case $r_t \to r$. The frontal illuminated area of the tube was in our model considered to be $4r_t r$. This holds when $r_t \ll r$ but when the tube radius is just as large as the radius of the illumination area, the illuminated area of the tube will be $\pi r_t^2 = \pi r^2$, while our model would give $4r_t^2 = 4r^2$. This makes Eq. 39 come out $4/\pi$ to high when $r_t = r$. So the 4 comes from the tube area, the π from the illumination area, and they are in the right place when the tube is small (giving just the right ratio when it becomes large), which it is in the experiments. However, in the limit $r_t \to r$, the transmittance factor between brackets cannot be correct, since then all the light should be passing through the tube regardless of its location, adding to the point made in the previous paragraph that Eq. 39 is cannot yet give a fully satisfying explanation of what happens in the slab.

Eq. 39 also indicates that the fraction of light passing through the tube decreases when the illumination area radius r is increased, or the tube radius is decreased, which makes sense – light will have ‘more ways’ to pass beyond the tube without entering it, until in the limiting case where $r_t/r \to 0$ the tube really becomes negligible and the fraction of dynamically scattered light to the overall detected power becomes zero. On the other hand, the equation is certainly not applicable to the case where $r_t > r$ or even in the same order of size, as already became clear in the previous

In the derivation of Eq. 39 throughout this chapter, some simplifications and assumptions were made which must be taken into account when considering its applicability.

First of all, the geometry was considered infinite in the directions perpendicular to the z-axis (Fig. 1) so one-dimensional diffusion could be used. In the experiment an illumination area with a diameter of approximately 2 centimeters (top hat profile) was used, while the sample thickness was 1 cm. Since the illuminated area diameter is not that much larger than the sample thickness, it can be expected that one-dimensional diffusion holds only to first approximation and better results can be obtained (though the calculations will become more involved) by looking at the true three-dimensional geometry. A lot has been written about diffusion and the so-called banana-shaped regions of photon migration path density between a source and detector for various geometries[15-19]. This could offer a more realistic approach. Monte Carlo simulations could bring more clarity to investigating these photon path distributions.

As a second approximation, absorption was neglected. Though it holds for Delrin that the absorption coefficient is much smaller than the reduced scattering coefficient[11], it remains to be seen whether absorption is really negligible. Taking into account absorption will give a different energy density profile and flux, and will therefore probably alter the result of Eq. 39.

Third, some approximations have been done regarding the tube. First of all, the scattering coefficient inside the tube was implicitly taken the same as outside, because the energy density and flux profiles inside the slab (so also across the tube) were calculated using one single value for the diffusion constant *D*, which is dependent on the mean free path length *l*, which is in turn the inverse of the reduced scattering coefficient. This approximation will hold well in the limit of a very small tube, since in this case the overall energy density and flux profiles will not be altered much by the presence of the tube even if *D* would be slightly different. It was already argued that our model cannot be expected to hold in the large tube limit.

Regarding the tube, there has also been a second tube approximation: regarding the tube as a point source. Discussion has been going on about the validity of this approach. The most vulnerable point seems to be the fact that in a real size tube, part of the light coming from the tube will re-enter it, and part of that light will re-enter it a second time, and so on. This light coming in a second or third time increases the amount of light going into the tube, but it does not increase the amount of time-dependent intensity detected, because it was already time-dependent from the first time it entered. To tackle this problem, as a first approximation, the amount of light entering the tube for the first time was considered to be given by the normal component of the flux (Eq. 34). This should account for the light passing through multiple times while being already dynamically scattered – but it would give much clarity if one would find a way to find the return probability p_r (Eq. 33). Even better would be to find a way to surpass the point source approximation and carry out the calculation for a real-size tube, also taking into account the amount of time spent in the tube (which is to say, the amount of scattering events with a moving scatterer) as a measure of to what amount light entering the tube will actually be dynamically scattered.

2.2 Calculating the normalized temporal intensity autocorrelation function

The aim of this subsection is to find an expression for the normalized temporal intensity autocorrelation function $g^{(2)}(\tau)$ – because intensity is what a camera detects – in terms of the electric field autocorrelation function $G(\tau)$. Similar approaches in literature can be found in references 2, 3, 4 and many others.

2.2.1 Simple derivation

The intensity of light is given by the square of the electric field amplitude:

$$I(t) = |E(t)|^2 = E(t)E^*(t), \tag{40}$$

where *E* is the electric field. When light diffuses through the slab to the other side, only part of the light will diffuse through the tube (and thus through the dynamic part of the sample), while another part of the light will experience only static scattering events. Hence, the electric field consists of a part that varies in time and a relatively stable (time-independent) part:

$$E(t) = A + B(t). \tag{41}$$

The (normalized) autocorrelation function of the intensity can be expressed as

$$g^{(2)}(\tau) = \frac{\langle I(t)I(t+\tau)\rangle}{\langle I(t)\rangle\langle I(t+\tau)\rangle}, \tag{42}$$

where the $\langle\ \ \rangle$ denote time average values. Because of the time averaging, $\langle I(t+\tau)\rangle = \langle I(t)\rangle$, and Eq. 42 can be written as

$$g^{(2)}(\tau) = \frac{\langle I(t)I(t+\tau)\rangle}{\langle I(t)\rangle^2} = \frac{\langle E(t)E^*(t)E(t+\tau)E^*(t+\tau)\rangle}{\langle E(t)E^*(t)\rangle^2}. \tag{43}$$

Inserting the expression for *E*(t) from Eq. 41 and working out some products and averages gives:

$$g^{(2)}(\tau) = \frac{\langle\left(|A|^2 + |B(t)|^2 + AB^*(t) + A^*B(t)\right)\left(|A|^2 + |B(t+\tau)|^2 + AB^*(t+\tau) + A^*B(t+\tau)\right)\rangle}{\langle|A|^2 + |B(t)|^2 + AB^*(t) + A^*B(t)\rangle^2}$$

$$= \frac{|A|^4 + |A|^2(\langle|B(t)|^2\rangle + \langle|B(t+\tau)|^2\rangle) + |A|^2(\langle B^*(t)B(t+\tau)\rangle + \langle B(t)B^*(t+\tau)\rangle) + \langle|B(t)|^2|B(t+\tau)|^2\rangle}{(|A|^2 + \langle|B(t)|^2\rangle)^2},$$

where the terms averaging to zero (because they have a time-dependent phase) have been left out. Again noting that $\langle B(t+\tau)\rangle = \langle B(t)\rangle$ and that

$$\langle B^*(t)B(t+\tau)\rangle = \langle B(t)B^*(t+\tau)\rangle \equiv \langle|B(t)|^2\rangle|G(\tau)|, \tag{44}$$

with G the so called intermediate scattering function, the equation simplifies to

$$g^{(2)}(\tau) = \frac{|A|^4 + 2|A|^2\langle|B(t)|^2\rangle + |A|^2\langle|B(t)|^2\rangle|G(\tau)| + \langle B(t)B^*(t+\tau)B^*(t)B(t+\tau)\rangle}{(|A|^2 + \langle|B(t)|^2\rangle)^2}$$

$$= \frac{|A|^4 + 2|A|^2\langle|B(t)|^2\rangle(1 + |G(\tau)|) + \langle|B(t)|^2\rangle^2(1 + |G(\tau)|^2)}{(|A|^2 + \langle|B(t)|^2\rangle)^2}, \tag{45}$$

where $\langle B(t)B^*(t+\tau)B^*(t)B(t+\tau)\rangle = \langle|B(t)|^2\rangle^2(1+|G(\tau)|^2)$ is used, as was shown by Boas[2]. This function can be written in terms of intensities by writing the time average of I as I_0 and evaluating it in terms of the field:

$$\begin{aligned} I_0 \equiv \langle I(t)\rangle &= \langle E(t)E^*(t)\rangle = \langle|A|^2 + |B(t)|^2 + A^*B(t) + AB^*(t)\rangle \\ &= |A|^2 + \langle|B(t)|^2\rangle = (I_0 - I_{sc}) + I_{sc}\,, \end{aligned} \tag{46}$$

where $I_{sc} \equiv \langle|B(t)|^2\rangle$ denotes the intensity arising from light that was scattered by moving scatterers (or said differently, by light that diffused through the tube). With these definitions, Eq. 45 becomes:

$$\begin{aligned} g^{(2)}(\tau) &= \frac{(I_0 - I_{sc})^2 + 2(I_0 - I_{sc})I_{sc}(1+|G(\tau)|) + I_{sc}^2(1+|G(\tau)|^2)}{I_0^2} \\ &= 1 + \frac{2(I_0 - I_{sc})I_{sc}|G(\tau)| + I_{sc}^2|G(\tau)|^2}{I_0^2}. \end{aligned} \tag{47}$$

This is an expression for the normalized temporal autocorrelation function.

2.2.2 Setup dependence

In reality, the decorrelation will be setup-dependent; it is shown by Boas and by Bonner and Nossal that a true physical setup will introduce a coherence factor β (0 < β < 1) which is dependent on the number of speckles imaged and the optical coherence of the signal at the detector[2][3]. Taking into account this factor in the calculations and normalizing $g^{(2)}(\tau)$ so it starts from 1+β and drops to (at least) 1 gives[4]:

$$g_\beta^{(2)}(\tau) = 1 + \beta\frac{(I_0 - I_{sc})^2 + 2(I_0 - I_{sc})I_{sc}|G(\tau)| + I_{sc}^2|G(\tau)|^2}{I_0^2}. \tag{48}$$

The ratio between the two intensities I_0 and I_{sc} was derived in the previous section, namely:

$$\frac{I_{sc}}{I_0} = \frac{P_{trans,tube}}{P_{trans}} = \frac{4r_t}{\pi r}\left(\frac{z_e + z_t}{L + 2z_e}\right). \tag{49}$$

In the experiments, the tube was placed at $z_t = \frac{1}{2}L$, in which case Eq. 49 gives:

$$\frac{I_{sc}}{I_0} = \frac{P_{trans,tube}}{P_{trans}} = \frac{2r_t}{\pi r}, \tag{50}$$

and the normalized temporal intensity autocorrelation function can be written as:

$$g_\beta^{(2)}(\tau) = 1 + \beta\left(\left(1 - \frac{2r_t}{\pi r}\right)^2 + 2\left(1 - \frac{2r_t}{r}\right)\frac{2r_t}{r}|G(\tau)| + \left(\frac{2r_t}{r}\right)^2|G(\tau)|^2\right). \tag{51}$$

From this point on, this function will be referred to simply as $g^{(2)}(\tau)$. Remains to determine the intermediate scattering function $G(\tau)$. This will be the goal of the following subsection.

2.2.3 Discussion

In the above derivation of the function $g^{(2)}(\tau)$, time averages were used. In the experiments, speckle averages were measured. The question is whether it is safe to assume ergodicity in this case. Various articles seem to suggest this might not be the case[2][20-25]. In this case a thorough revisitation of the autocorrelation function is needed.

On the other hand, all ways to determine the autocorrelation function mainly influence the normalization – the dependence on the intermediate scattering function *G* remains more or less the same, and since this is the one determining the decorrelation time, this value should also remain the same.

2.3 Calculating the intermediate scattering function

In general, finding the intermediate scattering function $G(\tau)$ is a tedious procedure that depends on the specific geometry used and a varying scale of assumptions. In the past it has been done for various situations, although – to our knowledge – not for the specific geometry of the experiments described in this report. However, some of the models might still be suitable to describe what is happening in our experiment to a reasonable degree of accuracy, or at least qualitatively. In this subsection, two of these models based on different routes to find $G(\tau)$ will be considered; one will follow the approach generally encountered in Laser Doppler Flowmetry situations, where the other will be based on (Multispeckle) Diffusive Wave Spectroscopy. An interesting paradox arises when it comes to the influence of particle movement, which will be described in the end of this subsection.

2.3.1 Intermediate scattering function used in Laser Doppler Flowmetry

A model for doing Laser Doppler Flowmetry (LDF) measurements on tissue was published by Bonner and Nossal in 1980[3]. They considered the perfusion of blood in tissue. The tissue was considered stable, while the blood flowed through many small vessels in random directions. They showed that, in general:

$$G(\tau) = \sum_{m=1}^{\infty} \frac{P_m G_m(\tau)}{1 - P_0}, \tag{52}$$

where $G_m(\tau)$ is the ISF for photons which experience *m* collisions with moving scatterers, and P_m is the probability that a particular photon will indeed experience *m* such collisions. They also showed, based on a result from Sorensen[6], that every $G_m(\tau)$ can be written in terms of $G_1(\tau)$, the ISF for photons that experience only one dynamic scattering event:

$$G_m(\tau) = |G_1(\tau)|^m, \tag{53}$$

so the resultant ISF is given by

$$G(\tau) = \sum_{m=1}^{\infty} \frac{P_m |G_1(\tau)|^m}{1 - P_0}. \tag{54}$$

This result is still completely general. Then they argued that the chance on m collisions, P_m, in their case would be a Poisson distribution:

$$P_m = \frac{\bar{m}^m e^{-\bar{m}}}{m!}, \tag{55}$$

where $\bar{m}$ is the mean number of collisions with a moving scatterer. This led them to the intermediate scattering function in the form:

$$G(\tau) = \frac{e^{\bar{m}(G_1(\tau)-1)} - e^{-\bar{m}}}{1 - e^{-\bar{m}}}. \tag{56}$$

Assuming this equation holds also for the experiments described in this report, there is still need to find a realistic value for $\bar{m}$. As a very rough first approximation, one could assume that

$$\bar{m} = \frac{1}{2}\left(\frac{2r_t}{l}\right)^2 = 2\left(\frac{r_t}{l}\right)^2, \tag{57}$$

because the mean number of collisions for light going through a slab of thickness L is $\frac{1}{2}\left(\frac{L}{l}\right)^2$. It must be noted that this only holds when *L* is much larger than the free path length *l* through the fluid.

Bonner and Nossal also worked out an equation for $G_1(\tau)$, which was valid for the case where the moving scatterers only underwent Brownian motion. Binzoni, Leung, Seghier and Delpy elaborated on their results, incorporating translational velocity into their model[4][5]. They found the following approximation for $G_1(\tau)$:

$$\begin{aligned} G_1(\tau) &\approx \frac{1}{\pi}\frac{12\xi a^2}{12\xi a^2 + \langle V_{brown}^2\rangle\tau^2}\int_0^\pi e^{\left[-\frac{3}{2}\frac{V_{trans}^2 \sin(\theta')^2\tau^2}{12\xi a^2+\langle V_{brown}^2\rangle\tau^2}\right]} d\theta' \\ &= -\frac{8\gamma\xi a^2}{V_{trans}^2\tau^2} e^{\gamma/2}\mathbf{I}_0\left(\frac{-\gamma}{2}\right), \end{aligned} \tag{58}$$

with $\mathbf{I}_0$ the modified Bessel function of the first kind of order 0 and

$$\gamma = -\frac{3}{2}\frac{V_{trans}^2\tau^2}{12\xi a^2 + \langle V_{brown}^2\rangle\tau^2}. \tag{59}$$

In these expressions, *a* is the radius of the moving spherical scatterers and ξ is a geometrical parameter, which in their as well as in our situation is to good approximation $\xi = 0.1$ [reference]. V_{trans} denotes the translational speed, which is taken constant across the vessels (i.e. no flow profile considerations are done). $\langle V_{brown}^2\rangle$ is the mean square value for the Brownian motion velocity. Assuming a Maxwell velocity distribution for Brownian motion,

$$\langle V_{brown}^2\rangle = \frac{k_B T}{m^*}, \tag{60}$$

with k_B the Boltzmann constant and T the temperature, and where instead of the mass of the spherical scatterers the effective mass m* is used[7][8], given by

$$m^* = \frac{4}{3}\pi a^3(\rho_{part} + 0.5\rho_{liq}). \tag{61}$$

Here ρ_{part} and ρ_{liq} are the densities of the particle and the surrounding liquid, respectively.

So with the above assumptions (Poisson distribution for P_m, constant V_{trans} across the vessels, tube modeled as a slab to find $\bar{m}$), the following equations define the ISF:

$$G(\tau) = \frac{e^{2\left(\frac{r_t}{l}\right)^2 (G_1(\tau)-1)} - e^{-2\left(\frac{r_t}{l}\right)^2}}{1 - e^{-2\left(\frac{r_t}{l}\right)^2}} \tag{62}$$

$$G_1(\tau) = \frac{12\xi a^2}{12\xi a^2 + \langle V_{brown}^2 \rangle \tau^2} e^{\left[-\frac{3}{4}\frac{V_{trans}^2 \tau^2}{12\xi a^2 + \langle V_{brown}^2 \rangle \tau^2}\right]} \mathbf{I}_0 \left(\frac{3}{4}\frac{V_{trans}^2 \tau^2}{12\xi a^2 + \langle V_{brown}^2 \rangle \tau^2}\right). \tag{63}$$

It cannot be expected that this model gives a very accurate description of the system, but it gives some hints about the relevant parameters.

Discussion of the LDF model

In deriving the intermediate scattering function, Eq. 56:

$$G(\tau) = \frac{e^{\bar{m}(G_1(\tau)-1)} - e^{-\bar{m}}}{1 - e^{-\bar{m}}}, \tag{56}$$

a Poisson distribution for the chance on m dynamic scattering events was used. This might hold for the case of blood perfusion, where there are many randomly oriented small vessels protruding the tissue; in the case described in this study of a single relatively large 'blood vessel', it can hardly be expected to hold. So a better relation between G and G_1 should be derived for this model to make more sense.

Secondly, the mean number of dynamic scattering events was calculated using

$$\bar{m} = \frac{1}{2}\left(\frac{2r_t}{l}\right)^2 = 2\left(\frac{r_t}{l}\right)^2, \tag{57}$$

as if the cylinder was a slab. This neglects the tube geometry, but more importantly, it neglects the fact that light is entering multiple times.

2.3.2 Intermediate scattering function used in Diffusing Wave Spectroscopy

In DWS, one usually looks at the speckle arising from laser light propagating through a homogeneous, fully dynamic medium, like a cuvette with some fluid inside. Also in this model, the ISF is largely dependent on the geometry used. Pine, Weitz, Chaikin and Herbolzheimer found the ISF for transmission through an infinitely large slab to be[9]

$$G(\tau) \approx \frac{\frac{L}{l}\sinh\left(\sqrt{\frac{6\tau}{\tau_0}}\right)}{\sinh\left(\frac{L}{l}\sqrt{\frac{6\tau}{\tau_0}}\right)}. \tag{64}$$

Here τ_0 is a characteristic time scale given by

$$\tau_0 = \frac{\lambda^2}{4\pi^2 D_f}, \tag{65}$$

where λ is the wavelength of the light and D_f is the diffusion constant of the fluid; according to the Stokes-Einstein relation[28], which holds in the low Reynolds number limit, it is given by

$$D_f = \frac{k_B T}{6\pi\eta a}, \tag{66}$$

where k_B is Boltzmann's constant, T is the temperature, a is again the radius of the scatterers and η is the dynamic viscosity, so

$$\tau_0 = \frac{3\eta a\lambda^2}{2\pi k_B T}. \tag{67}$$

The ISF mentioned above is again not very suitable for accurate predictions, since it is assumed again that the tube is a slab; this violates the true geometry, and it also neglects the possibility that light diffuses out of the tube and back into it a second time (or third, or more). Also, this model does not incorporate translational velocity. Still it might give hints about the time scale on which processes happen (particularly with low or no flow speed), and the parameters that play a role. Most notably, in this model, the viscosity and the laser wavelength play a role, while they do not appear in the Binzoni model[4][5], since there only the rms Brownian motion velocity is taken into account, which is viscosity-independent (Eq. 60).

Discussion of the DWS model

In this model the assumption made is again the one of geometry; the tube was treated as a slab so a known equation for $G(\tau)$ could be used. Deriving a similar equation for a cylinder and then using some kind of power series to compensate for the light entering multiple times would probably give a much better result out of this model, suitable for qualitative and maybe even quantitative predictions.

2.3.3 Discussion: paradox between the LDF and DWS models

The above two models give rise to interesting questions, since they are not nearly the same. One would, after all, expect that the LDF model for a case of high perfusion would look a lot like the DWS model. One of the most intriguing differences might be the appearance of the dynamic viscosity in the latter, while in the first it is not present. In the LDF model, only the rms velocity for Brownian motion appears (Eq. 60):

$$\langle V_{brown}^2 \rangle = \frac{k_B T}{m^*}. \tag{60}$$

This might seem reasonable in the case of Laser Doppler measurements, since it is the instantaneous velocity of the particles that cause the Doppler shifts measured. But thinking about the variation in time of speckle patterns, one could also argue that it is the displacement of the spherical scatterers that matters: the size of speckle inside the material is about half a wavelength, so it would be expected that the typical time scale for decorrelation would be the time it takes for particles to travel such a distance. This can be calculated by diffusion theory which states that[32]

$$\overline{x^2}(t) = \frac{k_B T}{3\pi\eta a} t, \tag{68}$$

where $\overline{x^2}$ is the nett average squared displacement of a particle. Putting $x = \frac{1}{2}\lambda$ gives a typical decorrelation time scale of

$$\tau_0 = \frac{3\pi\eta a \lambda^2}{4 k_B T}, \tag{69}$$

which scales linearly with the viscosity and with the square of the wavelength, just like in the DWS model (actually, it is the same τ_0 as in Eq. 67, apart from a factor $\pi^2/2$).

Speaking about wavelength, even when analyzing Doppler shifts, one would expect a dependence on the laser wavelength. To see why, consider the change in optical frequency because of a Doppler shift from reflection of a moving particle. Simplifying to one dimension, the frequency shift is proportional to the incoming frequency, and thus to the inverse of the wavelength:

$$\Delta\beta = \left(\frac{c - v_p}{c + v_p}\right)\beta_0 = \left(\frac{c - v_p}{c + v_p}\right)\frac{2\pi c}{\lambda}, \tag{70}$$

with v_p the particle velocity, $\Delta\beta$ is the change in angular frequency and β_0 is the angular frequency of the incoming light. It can be seen that the Doppler shift is wavelength dependent (in the three-dimensional case there are some angle factors, but the wavelength dependence remains). The Doppler shifts inside the medium give rise to a detected intensity that is a function of optical frequency, $I = I(\beta)$. It can be shown[10][26] that the power spectrum $P(\omega)$ (where ω is the angular frequency of the speckle variation) measured in LDF is proportional to the autocorrelation of $I(\beta)$:

$$P(\omega) \propto \int_0^\infty I(\beta) I(\beta + \omega) d\beta, \tag{71}$$

so the power spectrum will also depend of the laser wavelength used. Since the temporal intensity autocorrelation function $g^2(\tau)$ is, according to the Wiener-Khinchin theorem, just the Fourier transform of the power spectrum, one would expect the wavelength dependence to pop up in the autocorrelation function equation as well. This raises questions about the validity of the LDF model.

And yet practically all LDF instruments use the original Bonner and Nossal theory that does not show this wavelength-dependence.

To get some clues on this paradox, it is good to consider the derivation of the original Bonner and Nossal model[3] and the subsequent LDF model[4] by Binzoni. In their original paper, Bonner and Nossal actually find a wavelength *dependent* ISF for photons experiencing one scattering event, $G_1(\tau)$:

$$G_1(\tau) = \frac{2\xi}{2\xi + T^2} \frac{1 - e^{-2\xi L^2} e^{-L^2 T^2}}{1 - e^{-2\xi L^2}}, \tag{72}$$

where

$$L = 2ka \tag{73}$$
$$T = \langle V^2 \rangle^{1/2} \tau / \sqrt{6} a. \tag{74}$$

However, they show that this becomes

$$G_1(\tau) = \frac{2\xi}{2\xi + T^2}, \tag{75}$$

which is independent of L and therefore the wavelength, in the limit $\xi L^2 \gg 1$. In practice, they show that for $\xi = 0.1$ this holds for $L \geq \sqrt{20}$; with a Helium Neon laser of which they unfortunately do not state the wavelength, this approximation holds when the diameter of the particles $a > 0.15$ µm. In that case, the correction from the L-dependent terms is less than 4% of the value of $G_1(\tau)$. For a red blood cell, $a \approx 2.8$ µm, so this approximation can be safely used, thereby eliminating wavelength dependence.

However, for the Binzoni model, which is an expansion of the Bonner and Nossal theory to include translational motion, things are not so simple. Where Binzoni and his coworkers derive their (different!) $G_1(\tau)$, they state they use the Bonner and Nossal approximation (letting L be large enough to eliminate wavelength dependence as above) simply by letting $k \to \infty$, but unfortunately they do not show why this is allowed. In a real experiment, certainly the wave number will not be infinite, and therefore there is a condition on the size of the particles which was found by Bonner and Nossal for their equation ($a > 0.15$ µm), but is not given by Binzoni et al. So it is hard to say whether this is a valid approach in their case.

Also, it must be noted that in our experiment, Intralipid is used which has an approximate bead size of 49 nm, much *smaller* than the 0.15 µm limit found by Bonner and Nossal. Therefore, in measurements with Intralipid, it is well possible that the predictions from the LDF model will not agree with experimental results.

2.4 Tube flow

Though the model of Binzoni does not consider the flow profile of moving scatterers[4][5] (they consider the translational flow speed to be constant everywhere) and the DWS model does not incorporate any translational velocity at all, it is still interesting to look at the profile of fluid flowing through a pipe, because it can give another hint about decorrelation time scales.

2.4.1 Upper limit of the decorrelation time

The size of speckle inside the medium is approximately ½ λ. So it should hold that there is maximum decorrelation (locally) when a scatterer has moved this distance or more (the size of the particles in Intralipid 10%, about 49 nm, is less than 10 time as big as the 532 nm wavelength of the laser light).

The Reynolds number for tube flow can be computed by

$$\mathrm{Re} = \frac{\rho \bar{V} d}{\eta}, \tag{76}$$

where ρ is the density, $\bar{V}$ the average velocity, d the tube diameter and η the viscosity. In the situations encountered in this research the Reynolds number is Re = 100 or less, while laminar tube flow holds up to a Reynolds number of Re ≈ 2100[34]. Thus, the flow can be expected to be laminar. Introducing a no slip boundary condition will give a parabolic flow profile as depicted in Fig. 7.

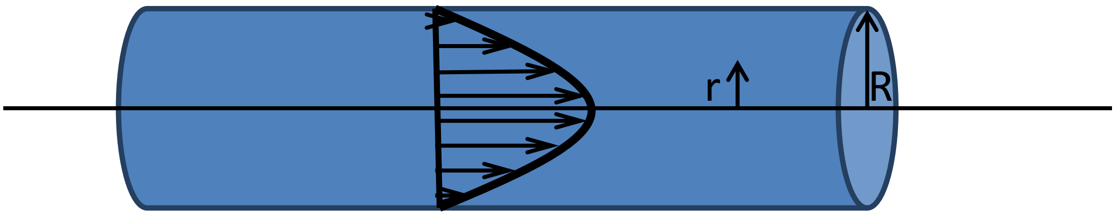

Figure 7. Parabolic flow of a fluid in a tube with no slip condition.

The profile can be computed by setting $v(R) = 0$ and $\left.\frac{\partial v}{\partial r}\right|_{r=0} = 0$:

$$\left.\begin{array}{l} v = c_1 r^2 + c_2 r + c_3 \\ v(R) = 0 \\ \left.\frac{\partial v}{\partial r}\right|_{r=0} = 0 \end{array}\right\} \Longrightarrow v = c_1(r^2 - R^2). \tag{77}$$

The constant c_1 can be found by integrating v over the tube cross-sectional area and putting it equal to the total discharge Q:

$$Q = \int v dA = \int_0^r \int_0^{2\pi} c_1(r^2 - R^2) r d\theta\, dr = -\frac{\pi c_1}{2} R^4 \Longrightarrow c_1 = -\frac{2Q}{\pi R^4}, \tag{78}$$

so the velocity profile becomes:

$$v = \frac{2Q}{\pi} \frac{R^2 - r^2}{R^4}. \tag{79}$$

To calculate at which time almost total decorrelation can be expected, a velocity v_{95} can be defined, as a velocity for which it holds that 95% of the liquid moves at least as fast as this. Because the velocity increases from the side to the middle of the tube, this must be the velocity at an r such that the area πr^2 is 95% of the total cross-sectional area πR^2:

$$v_{95} = v(r^2 = 0.95R^2) = \frac{0.1Q}{\pi R^2}. \tag{80}$$

Hence, the time it takes for 95% of the liquid to travel half a wavelength or more is:

$$t_{95} = \frac{\frac{1}{2}\lambda}{v_{95}} = \frac{\lambda \pi R^2}{0.2\,Q}. \tag{81}$$

It would be expected that after this time, further decorrelation due to translational movement is negligible. When Brownian motion is involved, true decorrelation time scales can be shorter still.

2.4.2 Discussion of tube flow considerations

Because the Reynolds number is well below 2700, the approximation of laminar flow will be valid. However, in the setup used in this study there is a change in tube diameter at the edge of the slab, where the exterior hoses for pumping the Intralipid are attached. This will cause some transit region which might actually be large enough to significantly change the flow profile in the investigated region. This might influence the time scales found, since it may cause a larger area where the fluid moves slower while moving faster on the inside. This will yield a value of t_{95} that is actually a bit too low. However, since this value is a serious overestimate of the decorrelation time, since no Brownian motion, no laser Doppler effects and only movements of half a wavelength or more were considered, it will probably still give a hint about the upper limit of possible decorrelation times.

2.5 Discussion and Conclusions

2.5.1 Recapitulation

In this chapter theory was partly developed and partly adapted from literature to find ways to predict the shape of the autocorrelation functions expected in our experiments, and, more specifically, the time scale on which decorrelation might take place. To get there, the following steps were taken:

1. Based on diffusion theory, a model was derived in section 2.1 to calculate the fraction of light transmitted through a slab of scattering material that went through a cylindrical tube inside; this fraction was found to be:
$$\frac{P_{trans,tube}}{P_{trans}} = \frac{4r_t}{\pi r}\left(\frac{z_e + z_t}{L + 2z_e}\right). \tag{39}$$
A number of approximations were made to arrive at this result, described throughout the text; the most important are:
    a. One-dimensional diffusion was considered to be appropriate for the case where the diameter of the illumination area is much larger than the thickness of the slab;
    b. The tube was considered much smaller than the illumination area cross-section, so that the energy density and flux profiles were not altered by the presence of a tube with liquid with a possibly different scattering coefficient than the sample;
    c. The power of light entering the tube for the first time was approximated by the normal component of the ingoing flux times the surface area;
    d. The (finite sized) tube was approximated as a point source radiating with this power.

    Assumption a. will be justified as long as the diameter of the illumination area is large enough; b. and d. would be expected to hold when the tube radius is small compared to the sample thickness, though it is hard to say how small would be sufficient. Assumption c. is a less obvious approximation, and it is expected that the model would be most improved if one would find a way around this point by finding the probability of light returning to the tube, and even better by finding a way to carry out the whole calculation of Eq. 39 for a finite-sized tube, not using the point-source approximation.
2. The normalized autocorrelation function $g^{(2)}(\tau)$ was calculated in section 2.2 along the lines followed by Boas[2], Binzoni[4] and others in terms of the ratio $I_{sc}/I_0 = P_{trans,tube}/P_{trans}$ found in step 1 and the intermediate scattering function $G(\tau)$. This function was found to be:
$$g_\beta^{(2)}(\tau) = 1 + \beta\,\frac{(I_0 - I_{sc})^2 + 2(I_0 - I_{sc})I_{sc}|G(\tau)| + I_{sc}^2|G(\tau)|^2}{I_0^2}, \tag{48}$$
in which the ratio $I_{sc}/I_0 = 2r_t/\pi r$ (for $z_t = \frac{1}{2}L$) can be inserted. Ergodicity was assumed, of which it is still unclear whether it holds or not[2][20-25].
3. The intermediate scattering function was determined in section 2.3 using two different models, one used in Laser Doppler Flowmetry and the other in Diffusing Wave Spectroscopy. In the LDF model, the intermediate scattering function was found to be:
$$G(\tau) = \frac{e^{2\left(\frac{r_t}{l}\right)^2 (G_1(\tau)-1)} - e^{-2\left(\frac{r_t}{l}\right)^2}}{1 - e^{-2\left(\frac{r_t}{l}\right)^2}}, \tag{62}$$
where $G_1(\tau)$ is the ISF for light experiencing only one dynamic scattering event, given by

$$G_1(\tau) = -\frac{8\gamma\xi a^2}{V_{trans}^2 \tau^2} e^{\gamma/2} \mathbf{I}_0\left(\frac{-\gamma}{2}\right), \tag{58}$$

where γ is defined in Eq. 59. Two notable approximations were made in deriving these results:

a. A Poisson distribution for the chance on m dynamic scattering events (Eq. 55) was used. This was actually derived for the case of a tissue with many microvessels, instead of a single larger vessel;
b. The tube was considered as a slab and the mean number of scattering events was estimated by the size of this slab divided by the mean free path length (Eq. 57), neglecting the fact that light might be entering multiple times.

A critical review of this model in the case of the setup used in our experiments is still needed. In the DWS model, the intermediate scattering function was found to be:

$$G(\tau) \approx \frac{\frac{L}{l}\sinh\left(\sqrt{\frac{6\tau}{\tau_0}}\right)}{\sinh\left(\frac{L}{l}\sqrt{\frac{6\tau}{\tau_0}}\right)}. \tag{64}$$

with τ_0 given by Eq. 67. This model does not take into account translational motion like the previous one. Furthermore, again an assumption very much like the second one of the LDF model was made: the tube was considered a slab, and the probability of light returning to it was not taken into account. Even so, since this model is being used to investigate Brownian motion in larger volumes of dynamic sample (also liquids), it might be more suitable for the situation in our experiments.

An interesting paradox, described in subsection 2.3.3, arose regarding wavelength dependence, that is present in the DWS model but not in the LDF model. In the derivation of the original LDF model without translational motion, it is argued why this dependence can be neglected, but in the expanded model (including translational motion) by Binzoni and others, this is not immediately clear.

4. In section 2.4, some fluid dynamics was used to find an expression for the time in which most of the fluid in the channel will have moved more than half a wavelength due to translational motion, the size of speckle inside the medium. It is therefore expected that after this time, practically no further decorrelation should take place, since the speckle inside will be decorrelated almost as much as it can be. The expression for this time was found to be:

$$t_{95} = \frac{\lambda\pi R^2}{0.2\,Q}. \tag{81}$$

The presence of Brownian motion would lower the time in which decorrelation takes place; Eq. 81 therefore gives an upper limit of decorrelation time scales. To arrive at this result, two notable assumptions were made:

a. The tube flow was considered laminar. This is a safe assumption, since the Reynolds number (about 100) is much lower than the condition for laminar flow (about 2100).
b. The flow profile was assumed parabolic. This will hold for laminar flow in a tube after initial effects from entering the tube have died out.

2.5.2 Outlook

A number of improvements can be imagined to the theory derived in this chapter.

First of all, the diffusion model to find the fraction of detected light that is dynamically scattered needs improvement. This can be achieved by various ways, already partly indicated in the discussion above; most complete would be a calculation using three-dimensional diffusion, a finite sized tube and a good estimate or even calculated value for the return probability of light escaping from the tube. As indicated, a lot was written about the density of photon paths and the characteristic banana-shaped regions that might prove helpful; on the other hand, Monte Carlo simulations might give values hard to find by calculation only. Experimentally, the influences of the tube size and the tube location on the amount of dynamically scattered light should be investigated to get more insight in the validity of Eq. 39.

Second, it would be good to investigate whether the derived autocorrelation function is correct; there are some slightly different autocorrelation functions found in literature. It is especially the way the parameter β is inserted that is not the same everywhere and was also not worked out in this report; a thorough derivation of this result is given by Boas[2].

Third, both the LDF and DWS models need to be adapted to be really applicable to the given experimental setup; the first one originally does not consider one large vessel in a stable medium, but many small ones, while the second was originally derived for a homogeneous sample (e.g. one piece of Delrin, or a cuvette of Intralipid) and does not include translational motion. In using both of these models, the tube was considered as a slab and the returning of light was not considered; if the return probability of light is known, this problem can also be solved.

A last interesting point to look at is the validity of the way the wavelength-dependence is cancelled out in the LDF model by Binzoni and others. As already touched upon above, and explained in section 2.3.3, it is not clear whether and under what conditions this approximation is valid.

Predictions from the theory developed in this chapter will be given in the beginning of the following chapter.

3. Experiment

3.1 Predictions from the different models

In the previous chapter, two different models were considered to find the intermediate scattering function $G(\tau)$, and thereby autocorrelation function $g^{(2)}(\tau)$:

$$g^{(2)}(\tau) = 1 + \beta\left(\left(1 - \frac{2r_t}{\pi r}\right)^2 + 2\left(1 - \frac{2r_t}{r}\right)\frac{2r_t}{r}|G(\tau)| + \left(\frac{2r_t}{r}\right)^2 |G(\tau)|^2\right). \qquad (51)$$

The models used to find $G(\tau)$ were the Laser Doppler Flowmetry model and the Diffusing Wave Spectroscopy model. Also, some considerations were made about the flow of liquid in a tube, resulting in a theoretical upper limit for speckle decorrelation times. In this subsection, these models will be evaluated with parameters approximating the values used in the real experiments to find predictions for the autocorrelation and the decorrelation time scales and to compare the different models.

3.1.1 Laser Doppler Flowmetry model

In the LDF model, the following equations describe the intermediate scattering function:

$$G(\tau) = \frac{e^{2\left(\frac{r_t}{l}\right)^2 (G_1(\tau)-1)} - e^{-2\left(\frac{r_t}{l}\right)^2}}{1 - e^{-2\left(\frac{r_t}{l}\right)^2}}, \qquad (62)$$

$$G_1(\tau) = \frac{12\xi a^2}{12\xi a^2 + \langle V_{brown}^2\rangle\tau^2} e^{\left[-\frac{3}{4}\frac{V_{trans}^2\tau^2}{12\xi a^2 + \langle V_{brown}^2\rangle\tau^2}\right]} \mathbf{I}_0\left(\frac{3}{4}\frac{V_{trans}^2\tau^2}{12\xi a^2 + \langle V_{brown}^2\rangle\tau^2}\right), \qquad (63)$$

where $G(\tau)$ is the ISF itself and $G_1(\tau)$ the ISF for light experiencing only one scattering event.

Fig. 8 shows plots of $G_1(\tau)$, $G(\tau)$ and the resulting $g_{LDF}^{(2)}(\tau)$ for a 10 mm thick Delrin sample with a 2.2 mm tube with Intralipid inside, which are the actual parameters of the sample used in the experiments. The mean free path lengths in Delrin and Intralipid are taken to be 0.1 mm and 0.3 mm, respectively[11-14]. The radius of the illuminated area is chosen to be 10 mm, which is also roughly the same as in the experiment. The particle radius was taken 49 nm which is a typical value for Intralipid[27], and the density of particle and liquid are taken as 917 and 1000 kg/m^3, respectively. These are normal fat and water densities. This gives a rms Brownian motion velocity of approximately

$$\sqrt{\langle V_{brown}^2\rangle} \approx 7.48 \cdot 10^{-2} \text{ m/s}.$$

The translational velocity was chosen to be 0 for the sake of comparison.

It can be seen from Fig. 8 that the intermediate scattering function for light experiencing only one scattering event $G_1(\tau)$ decreases from one to zero in time scales of about 10^{-6} s. The total intermediate scattering function $G(\tau)$ decreases faster – which would be expected, since multiple scattering events are now also involved – in time scales of about 10^{-8} s. The same time scales are seen in the normalized autocorrelation function of the speckle $g^{(2)}{}_{LDF}(\tau)$; the time it takes for the autocorrelation to reach half its peak value is:

$\tau_{1/2} \approx 1.252 \cdot 10^{-8}$ s.

Predictions for other flow speeds – relating to the discharges used in the experiments – are listed in Table 1 below and plotted in Fig. 9. For low flow speeds (0 – 0,01 m/s) the decorrelation times do not decrease very fast, because Brownian motion is still by far more significant in this region, as is suggested by the rms Brownian motion velocity found above. At higher speeds, the decorrelation times start to decrease faster until at speeds higher than about 0.08 m/s the rate of decrease starts to lower again, in the end approaching zero when the speed goes to infinity.

V_{trans} (x 10^{-3} m/s)	$\tau_{1/2}$ (x 10^{-8} s)
0	1.252
4.38	1.250
8.76	1.246
13.2	1.238
17.5	1.227
21.9	1.214
26.3	1.198
30.7	1.180
35.1	1.160
39.5	1.139

Table 1. half time for different translational velocities

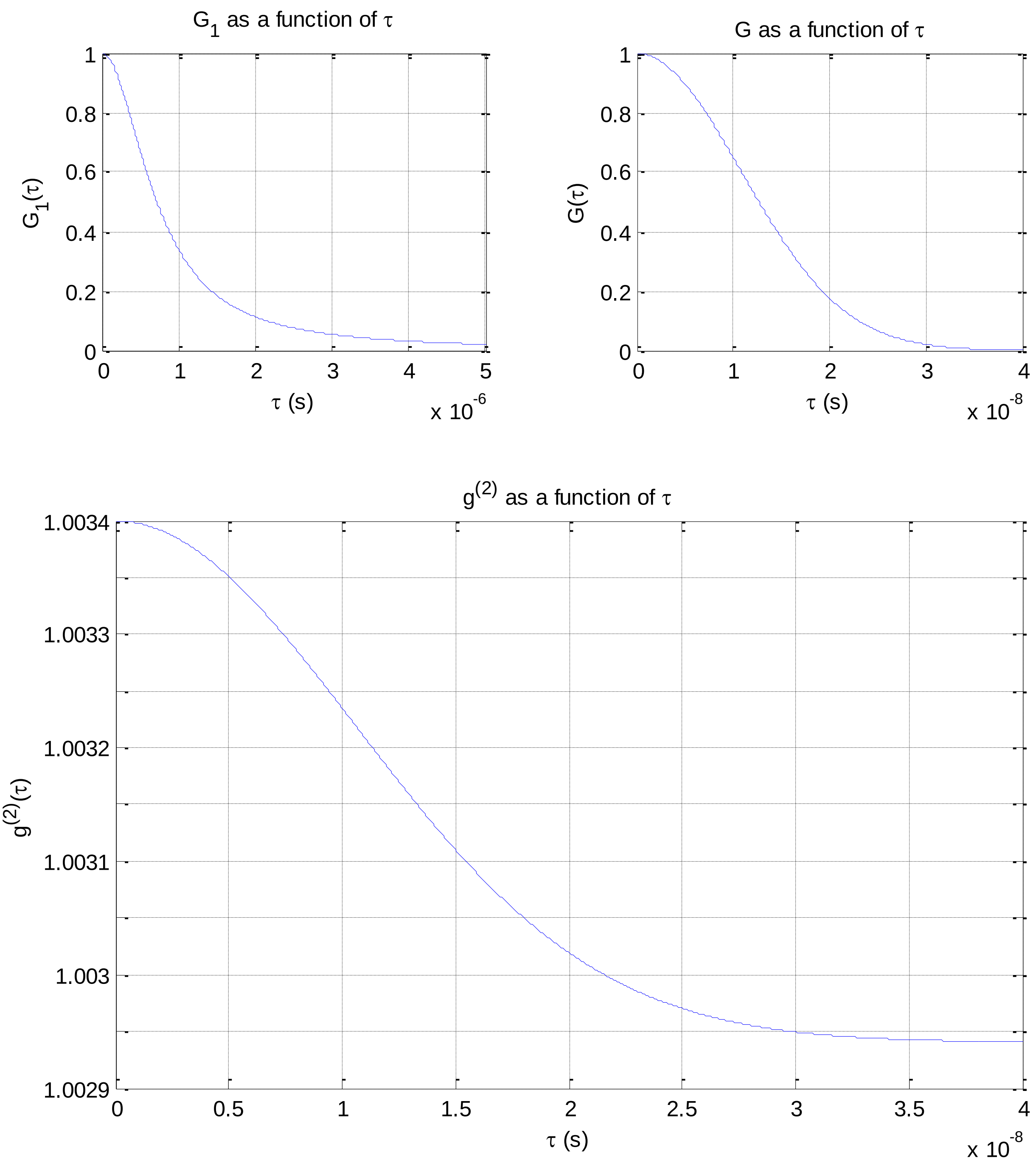

Figure 8. intermediate scattering functions $G_1(\tau)$ and $G(\tau)$, and the resulting $g^2_{LDF}(\tau)$ for the LDF model (zero translational velocity)

a)

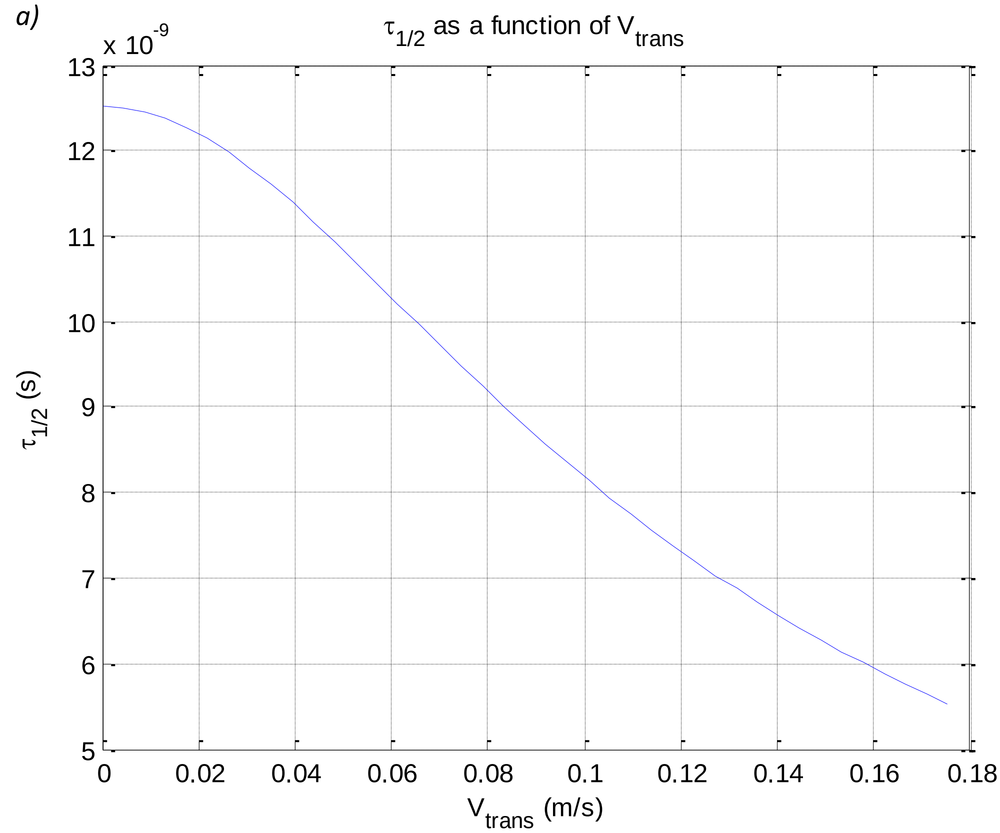

b)

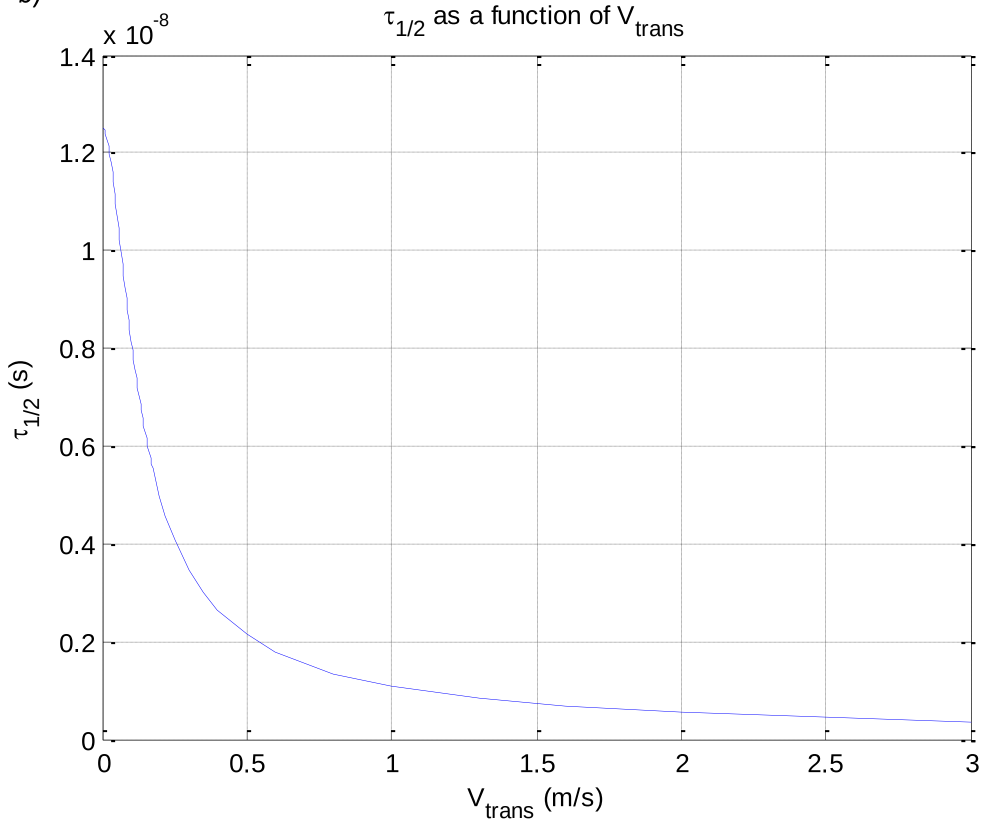

Figure 9. half time as a function of translational velocity. a) shows the region where translational motion starts to take over from Brownian motion; b) shows the decorrelation time on a larger V_{trans}-scale, approaching zero for large translational velocities.

3.1.2 Diffusing Wave Spectroscopy model

In the DWS model, the intermediate scattering function is given by

$$G(\tau) \approx \frac{\frac{L}{l}\sinh\left(\sqrt{\frac{6\tau}{\tau_0}}\right)}{\sinh\left(\frac{L}{l}\sqrt{\frac{6\tau}{\tau_0}}\right)}. \tag{64}$$

Fig. 10 shows plots of $G(\tau)$ and the resulting $g^{(2)}{}_{DWS}(\tau)$ for the DWS model, for the same parameters as described in the previous section. Instead of the viscosity of Intralipid, which is not documented well and often stock-dependent, the viscosity of water was used, which is actually usually very close to that of Intralipid. Because in the experiments the Intralipid comes from the refrigerator, the viscosity at 283 K was used ($\eta \approx 1.3$ mPa s).

The intermediate scattering function $G(\tau)$ in this situation again decreases from one to zero, but in a much slower way than in the previous model: the time scale is in the order of 10^{-5} to 10^{-4} s. The same holds for the autocorrelation function $g_{DWS}^{(2)}(\tau)$ itself. Where the previous model showed an almost horizontal slope in the beginning and subsequent decrease (Fig. 8), $g_{DWS}^{(2)}(\tau)$ starts to drop immediately.

According to this model, the time it takes for the autocorrelation to reach half its peak value is

$$\tau_{1/2} \approx 3.26 \cdot 10^{-5} \text{ s},$$

which is much larger than in the previous model (where it was $1.217 \cdot 10^{-8}$ s for zero translational velocity). As pointed out before, translational velocity cannot be taken into account in this model as it stands.

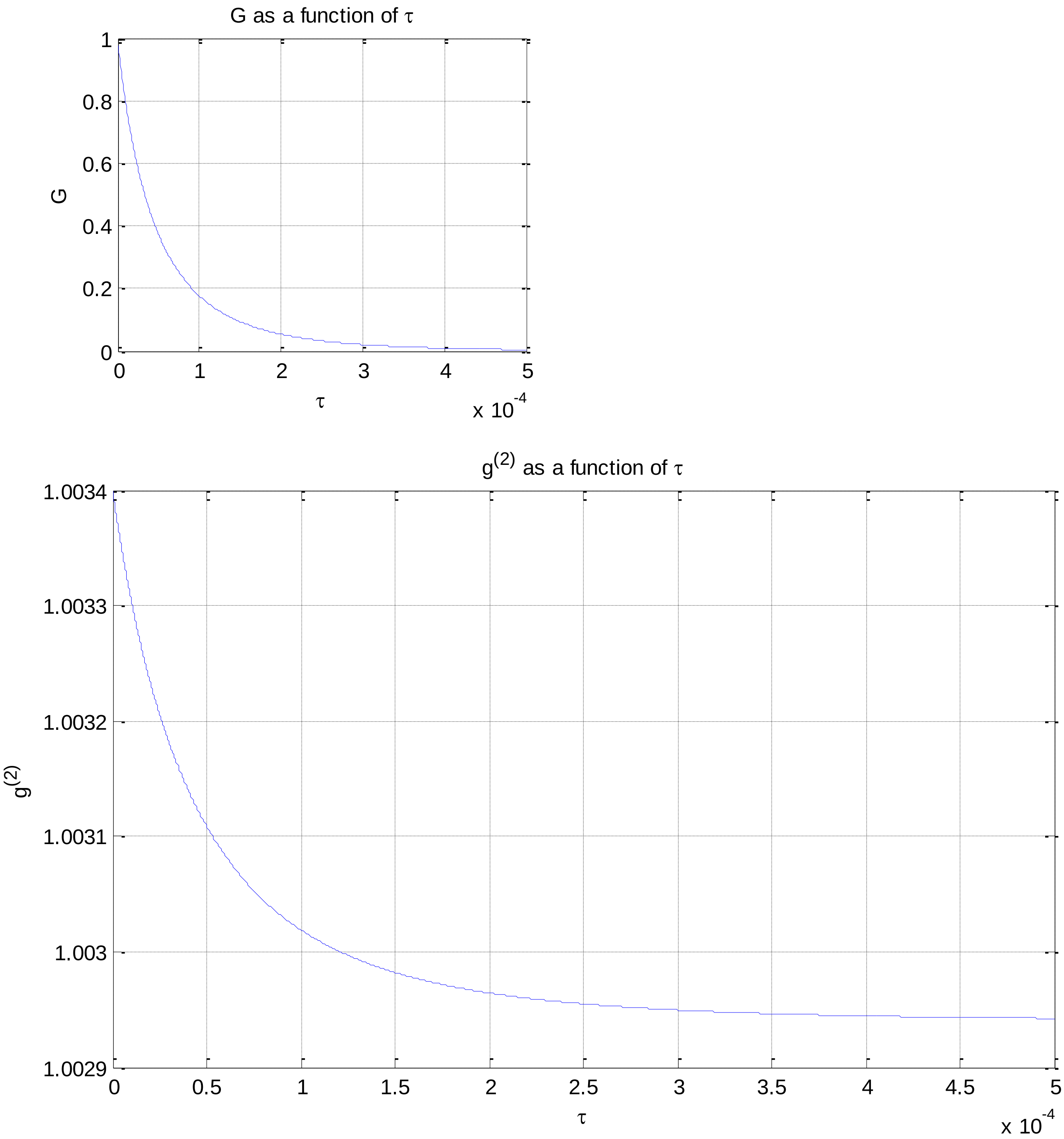

Figure 10. intermediate scattering functions G(τ), and the resulting $g^2_{DWS}(\tau)$ for the DWS model.

3.1.3 Tube flow

While the tube flow considerations do not directly offer a way to find the autocorrelation function or even the half time for the decorrelation, they do point to an upper limit for time scales on which decorrelation effects can take place due to translational velocity. This upper limit was found to be

$$t_{95} = \frac{\lambda \pi R^2}{0.2\,Q}. \tag{81}$$

After this time the speckle will certainly be almost totally decorrelated. For a tube radius of 1.1 mm and discharges used in the experiments, t_{95} ranges from 6.7 · 10^{-5} to 6.07 · 10^{-4} s (see also table 2 and Fig. 11). For a tube with diameter d = 3.2 mm, t_{95} ranges from 1.4 · 10^{-4} to 1.3 · 10^{-3} s in a similar fashion. It must be noted that these values are much larger than the decorrelation times found by using the LDF model. They cannot be compared directly to the DWS model, because that assumes only Brownian motion.

Q (ml/min)	**V_{trans} (x 10^{-3} m/s)**	**t_{95} (x 10^{-4} s)**
1.000	4.38	6.067
2.000	8.76	3.034
3.000	13.2	2.022
4.000	17.5	1.517
5.000	21.9	1.213
6.000	26.3	1.011
7.000	30.7	0.867
8.000	35.1	0.758
9.000	39.5	0.674

Table 2. values of t_{95} for typical discharge values

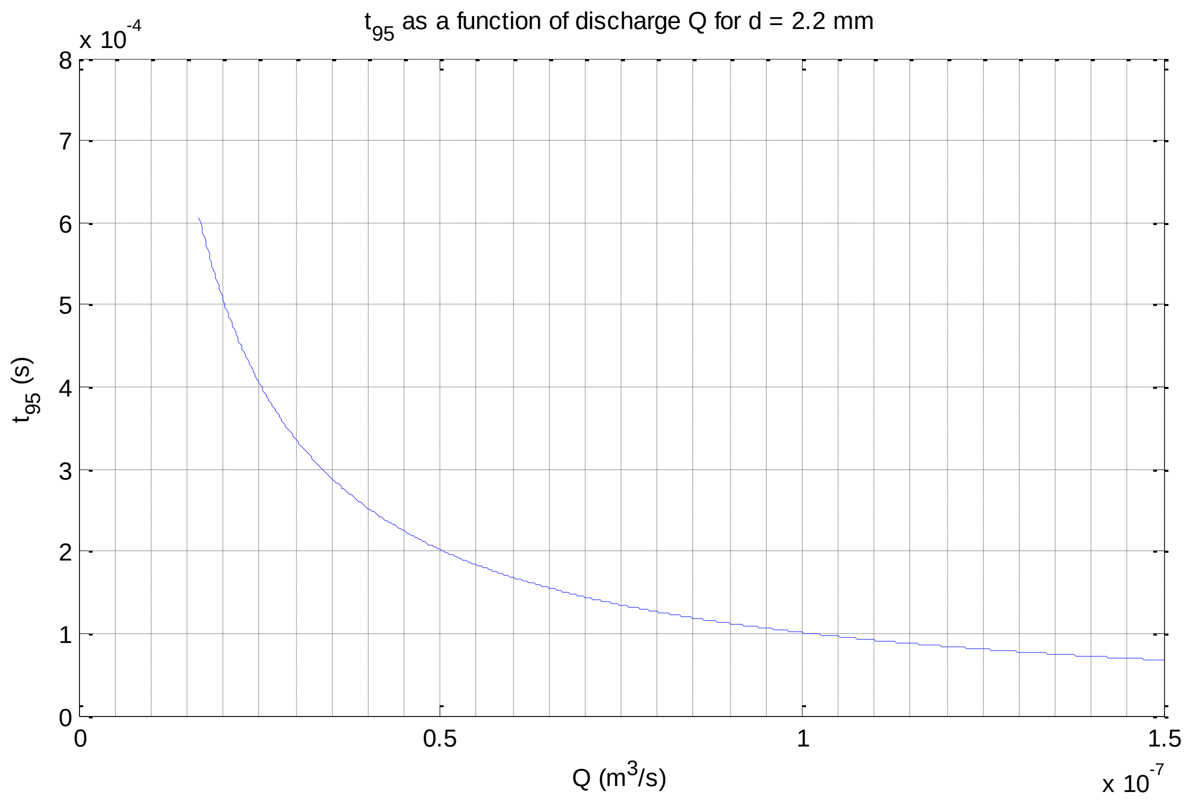

Figure 11. t_{95} versus discharge Q according to laminar tube flow considerations

3.1.4 Comparing the models

A direct comparison of the LDF and DWS models is only possible when one excludes translational motion, because it is not incorporated in the DWS model. The models give rise to a large difference in predictions. First of all, the time scales differ by a factor in the order of 10^4:

$$\tau_{1/2,LDF} \approx 1.217 \cdot 10^{-8}\ \mathrm{s}$$

$$\tau_{1/2,DWS} \approx 3.03 \cdot 10^{-4}\ \mathrm{s}$$

(zero translational velocity). It can also be noted that the shape of the autocorrelation curves (Fig. 8 and Fig. 10) are different, most notably because in the LDF model there is a plateau in the beginning of the curve, which is entirely absent in the DWS model.

When calculating the typical time scale on which decorrelation effects by Brownian motion take place (see 2.3.3 Paradox between the LDF and DWS models), a typical time of

$$\tau_0 = \frac{3\pi\eta a\lambda^2}{4k_B T} \tag{69}$$

was found, which is the same expression as that for the characteristic time found in the DWS model, apart from a factor $2/\pi^2 \approx 0.2$:

$$\tau_{0,DWS} = \frac{3\eta a\lambda^2}{2\pi k_B T}. \tag{67}$$

This makes the time scales found with the LDF model (for zero translational velocity) very unlikely, but it is more in agreement with the values found with the DWS model.

The calculations for laminar tube flow give maximal decorrelation time scale values for any chosen translational velocity. These are, for the velocities used in the experiments, in the order of 10^{-5} – 10^{-4} s (see Table 2), well above the half times found for in the LDF model, which are in the order of 10^{-8} s (Table 1).

3.2 Measurement set-up

In the Fig. 12 the measurement setup can be seen.

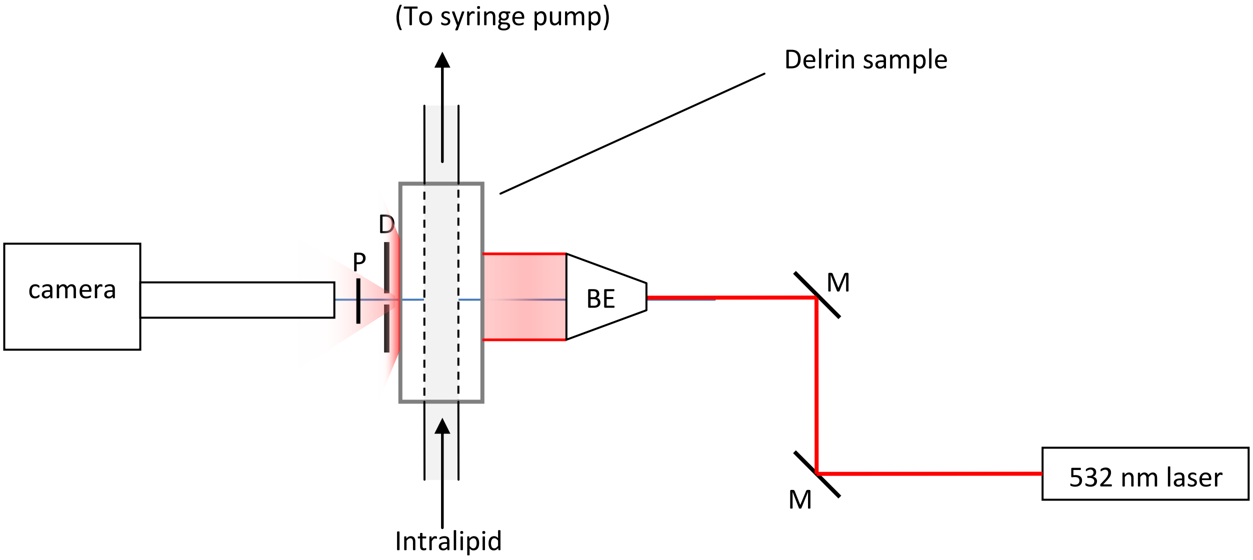

Figure 12. measurement setup. M, mirror; BE, beam expander; D, Diaphragm; P, polarizer.

A 532 nm diode laser beam is aligned by two mirrors. The light then enters a beam expander, which contains a microlens array that creates a 2 cm wide tophat intensity profile. This beam expander is used because the theoretical model is based on a plane wave. The light is then scattered by the sample. Just behind the sample there is a diaphragm so only a small part of the light will go the camera. The camera is a Photron Fastcam 1024PCI high speed camera that can measure up to 109500 frames per second. A polarizer is placed in front of the camera to increase the contrast of the speckle pattern.

The size of the speckle on the camera is[33]:

$$W = \frac{\lambda z}{D}, \tag{66}$$

where λ is the wavelength of the light, *z* is the distance between the sample and the camera and *D* is the size of the aperture where the light goes through after the sample (the diaphragm).In the measurements the speckle size was around 3 by 3 pixels.

The sample which is used is made of Delrin, which has scattering characteristics comparable to those of skin tissue. The reduced scattering coefficient of Delrin μ_s' = 2.3 mm^{-1} and the absorption coefficient μ_a = 0.002 mm^{-1}.[29] The absorption is low, so our approximation of no absorption is a good one. Two samples were used, one with a 2.2 mm and another with a 3.2 mm tube diameter. We used Intralipid 10 % as liquid to flow through the tube, thus imitating blood flowing through a blood vessel. Intralipid is an emulsion of fat droplets in water, with a reduced scattering coefficient of 6.8 mm^{-1} and an absorption coefficient of about 0.009 mm^{-1}. [12]

Intralipid needs to be stored in low temperatures, otherwise it will degrade. Also, the temperature can have influence on the scattering coefficient and on the amount of Brownian motion. To keep the Intralipid around 5 °C we put the Intralipid back in the fridge after each measurement.

The flow of Intralipid is driven by a syringe pump, which can be adjusted to different discharges. The pump sucks the Intralipid upwards towards the horizontal tube in the sample, through the tube and then further up towards the syringe.

3.3 Results

We took measurements for both samples for discharges of 0, 1, 2, 3, 4, 5, 6, 7, 8 and 9 ml/min. Also, we took control measurements with empty tubes (without Intralipid), one with the syringe pump off and one with the pump on to investigate the possible influence of vibrations of the pump engine on the speckle decorrelation. We took pictures with a frame rate of 45 kHz and a shutter time of 1/657000, the latter as low as possible to prevent blurring as much as possible.

For every pixel, we took the autocorrelation in time by using the Wiener-Khinchin Theorem, which connects the power spectrum and autocorrelation via a Fourier Transform. This means that first the power spectrum of one pixel in time can be calculated and then the inverse Fourier Transform can be taken to obtain the autocorrelation. The autocorrelation is then normalized by dividing through the mean intensity of that pixel in time:

$$g^{(2)} = \frac{\langle I(t)I(t+\tau)\rangle}{\langle I(t)\rangle^2} \tag{67}$$

After computing the autocorrelation function per pixel, an average autocorrelation function is obtained by taking the average of the autocorrelation functions of all pixels.

3.3.1 Results for a 2.2 mm diameter tube

In Fig. 13 and Fig. 14 below the autocorrelation functions of the measurement with a tube diameter of 2.2 mm can be seen. In Fig. 13 and Fig. 14 we see also some peaks, these are there only for the autocorrelation of no Intralipid and the pump on. The reason for these peaks is unknown.

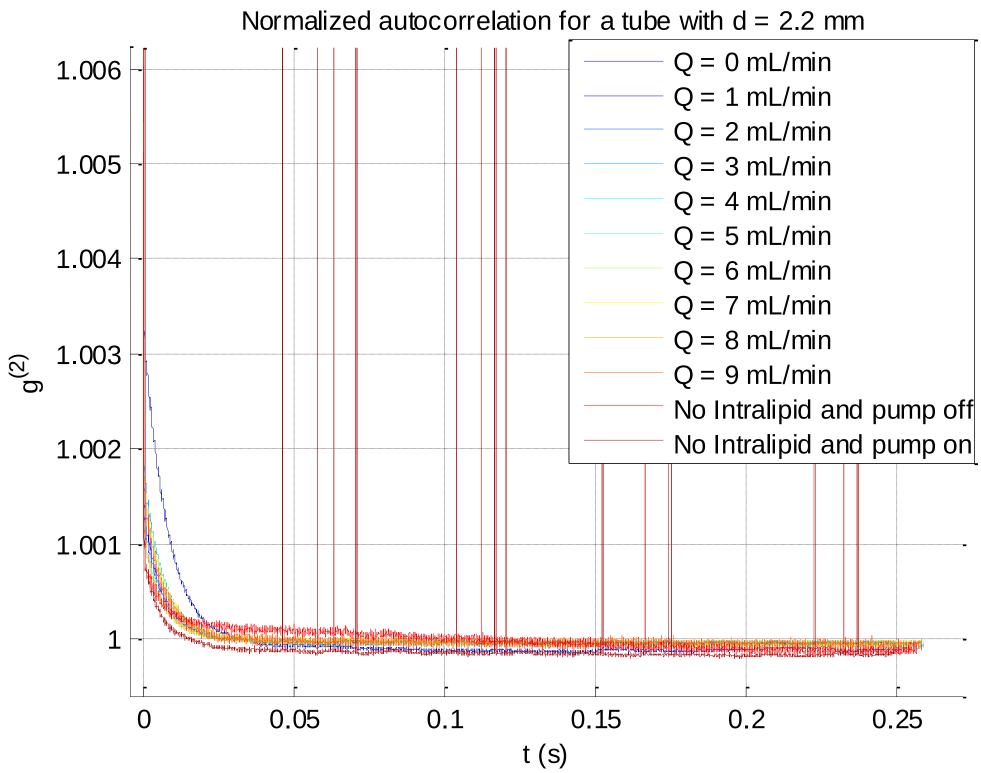

Figure 13. Autocorrelation functions of different discharges at a tube diameter of 2.2 mm

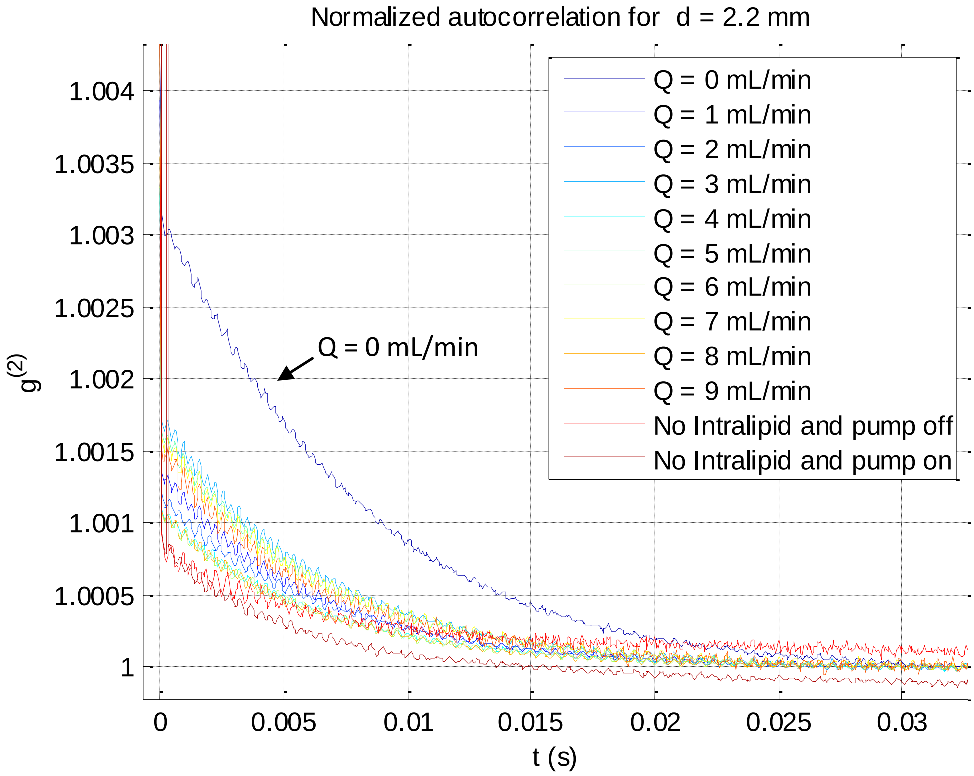

Figure 14. Autocorrelation functions of different discharges at a tube diameter of 2.2 mm

All autocorrelation functions have a sharp peak around time zero and then decrease to a value of about 1. The peak in the first data point can be caused by two effects. The first one is the presence of noise, which was not taken along in our normalization procedure. The second effect might be that processes take place in time scales shorter than the time between two camera frames (but still longer than the shutter time).

The autocorrelation functions of the sample without any fluid present show some slow decorrelation, which must be caused by instability of the sample or setup. Though it is hard to give a value for the half time because it is not known how much of the peak is caused by noise, it is clear that the half time for the sample with stationary fluid is shorter than with an empty tube. That there is more decorrelation in this situation will most likely be due to Brownian motion of the Intralipid beads.

The fact that the autocorrelation function seems to start higher for the tube with stationary fluid than that for the empty tube, can be caused by different effects. First, both the amount of noise and the amount of decorrelation between two frames can differ, the first caused by changes in intensity and the latter by Brownian motion. Second, the value of β, which should determine the offset, can also change. One of the reasons can be that some decorrelation takes place within the shutter time of the camera, causing the pictures to blur slightly. However, it is also the normalization procedure that influences this offset. When normalizing by dividing through $\langle I(t)\rangle^2$, an infinite measurement will approach a value of 1, but our finite time measurements end up having a mean value of 1. In equation 48, it can be seen that in theory the autocorrelation functions should vary from $1+\beta$ to $1+\beta[(I_0-I_{sc})/I_0]^2$, indicating that there is still a discrepancy between the theoretical and experimental normalization procedure. Still, it holds that the most reasonable explanation for the difference between the functions is the influence of Brownian motion.

The autocorrelation functions of all the other experiments, with discharges varying from 1 to 9 mL/min, seem randomly distributed, actually resembling the situation without any fluid more than that with stationary fluid. Apparently the speckle patterns seem to decorrelate less, while fluid is actually moving more. This could be explained by assuming that for these discharges, the decorrelation caused by translational velocity of the fluid is already so fast that a significant part of it takes place within the shutter time of the camera, causing the pictures to blur, so that decorrelation of the picture series will be less. This might leave the original sample decorrelation as dominant visible effect, like with the empty tubes. Indeed, contrast values of about 0.24 for empty tube experiments decreased to about 0.15 when Intralipid was present. On the other hand, no obvious difference between contrast values for different flow velocities (including zero) was found, which could indicate that Brownian motion alone already caused most of the blurring.

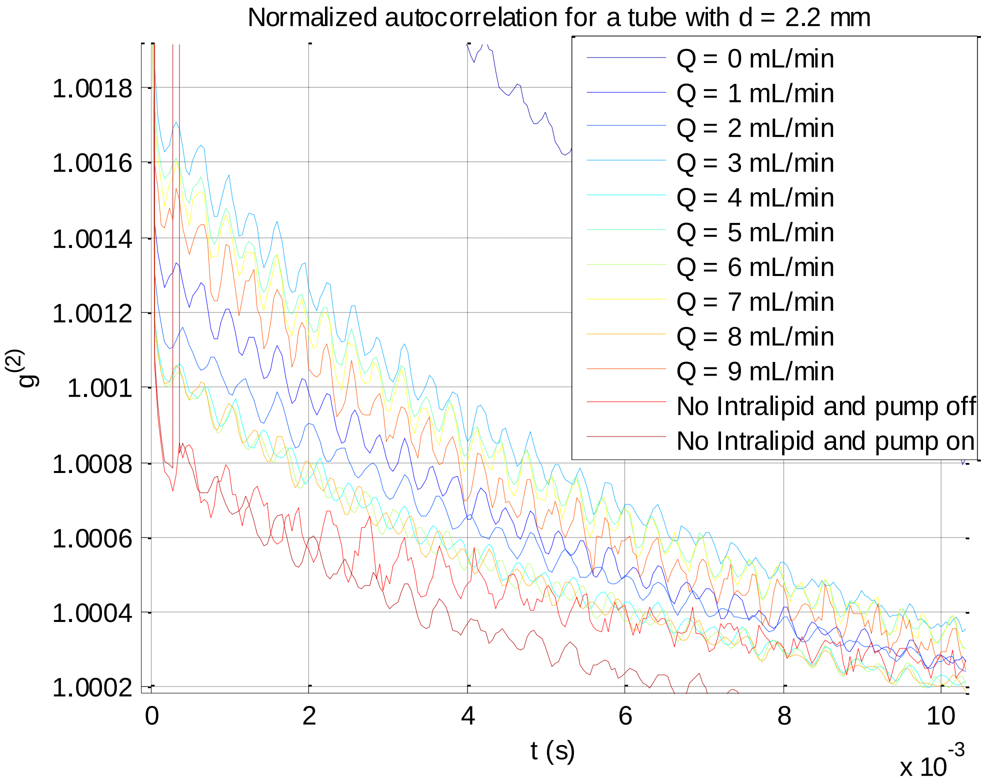

Figure 15. Autocorrelation functions of different discharges at a tube diameter of 2.2 mm

If we zoom in on the first 0.001 seconds we see some other things (Fig. 15). It can be seen that for the measurements with the empty tubes, the autocorrelation decreases fast in the beginning and then decreases just as fast as or a bit slower than the measurements with flowing Intralipid.

It can also be seen that there is a periodic signal in the autocorrelation functions. To study what frequency this signal has and whether this frequency is the same in all the measurements, we made a power spectrum of each discharge which can be seen in Fig. 16.

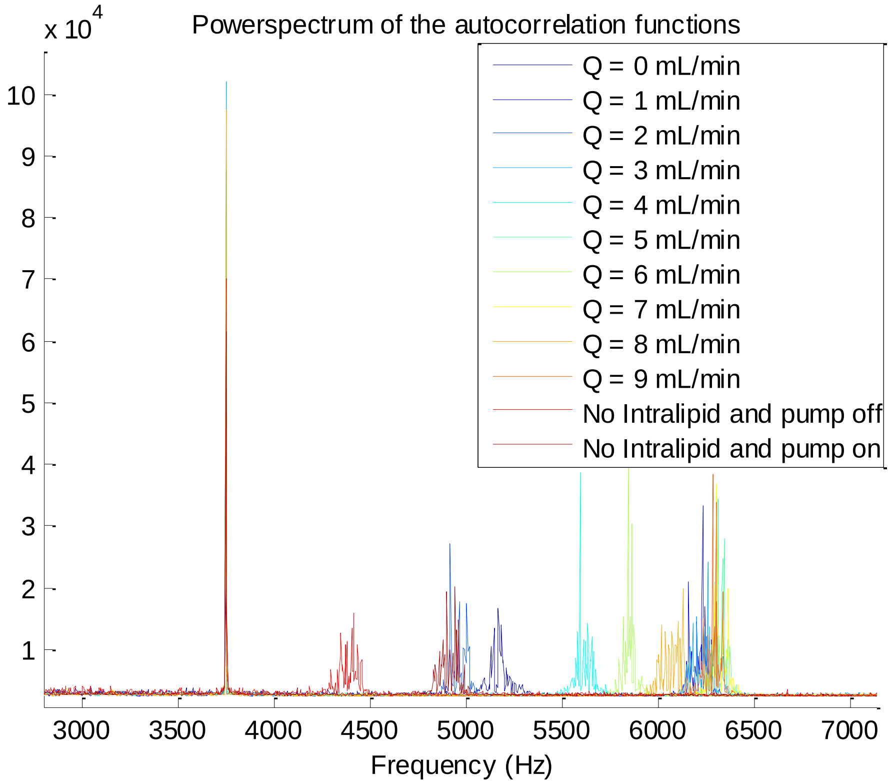

Figure 16.Powerspecturm of the intensity for different discharges at a tube diameter of 2.2 mm

In Fig. 16 it can be seen that all discharges have a peak around 3750Hz. This is not coming from the pump, because the peak is still there when the pump is off. We have not found out the reason behind this periodicity. For the other high frequency peaks it is also unclear, where they come from.

3.3.2 Results for a 3.2 mm diameter tube

We also took some measurements for a tube with a diameter of 3.2 mm. For the empty tube, so with no Intralipid the pump was off.

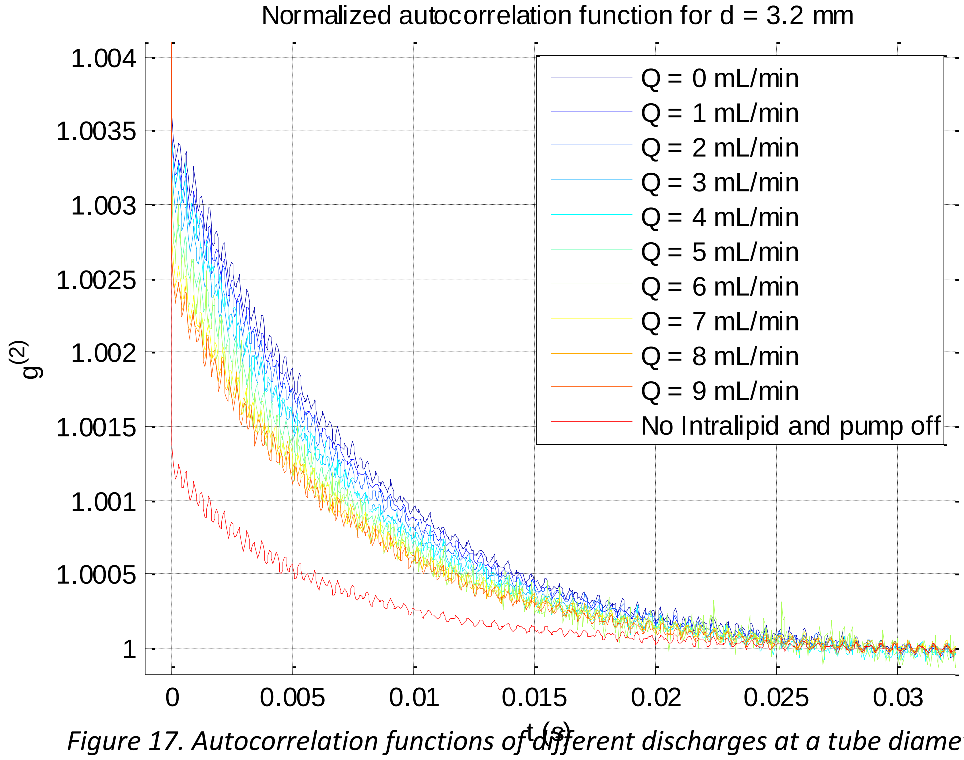

Figure 17. Autocorrelation functions of different discharges at a tube diameter of 3.2 mm

Fig. 17 is very different then the result found for d = 2.2 mm. It can be seen that if there is no Intralipid in the sample, the autocorrelation decreases less, which is logical because it is that is the most static situation. When there is Intralipid in the tube it decorrelates more, how lower the discharge is how more it decorrelates, Fig. 18 gives a good view on this. Actually one should expect that at higher discharge the speckle pattern will decorrelates more, but here it is the other way around. This is can be explained by assuming that the in the first two points the most decorrelation of the discharge is done. Therefore after the first two points the highest discharge has the lowest value at the autocorrelation function. The periodic signal which can be seen in the autocorrelations again has a frequency of about 3750 Hz.

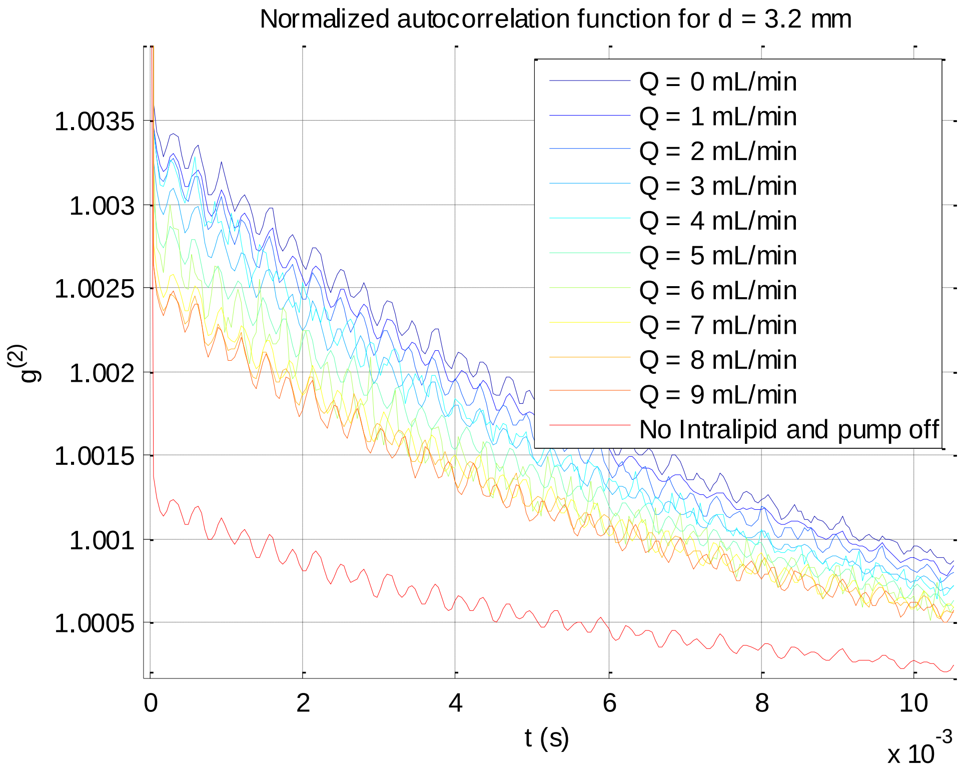

Figure 18. Autocorrelation functions of different discharges at a tube diameter of 3.2 mm

It is remarkable that the autocorrelation functions for a certain discharge are higher for d = 3.2 mm than for d = 2.2 mm. The reason for this can be that the translational velocity of the Intralipid is lower in the 3.2 mm tube than in the 2.2 mm tube for the same discharge, because the cross sectional area is larger. For d = 3.2 mm more light will pass through the tube, so the contribution of the dynamic part to the speckle pattern will also be higher. This makes the changes in the speckle pattern more notable, which increases decorrelation.

3.4 Analysis

3.4.1 The accuracy of the measurement

Unfortunately the measurements are only done once. This makes it difficult to say something about how much the autocorrelation can differ from the real function. Therefore we split up a measurement and calculated the autocorrelation function. For the measurement with Q = 1 mL/min and d =2.2 mm Fig. 19a is found. From this we see that the autocorrelation of 1 mL/min can differ at least this amount. Fig 19.b shows the autocorrelations functions from Fig. 14 for comparison. It can be seen that the autocorrelation functions can differ to different discharges, but it can be seen that the autocorrelation of the discharge Q = 0 mL/min is different than the for other autocorrelation.

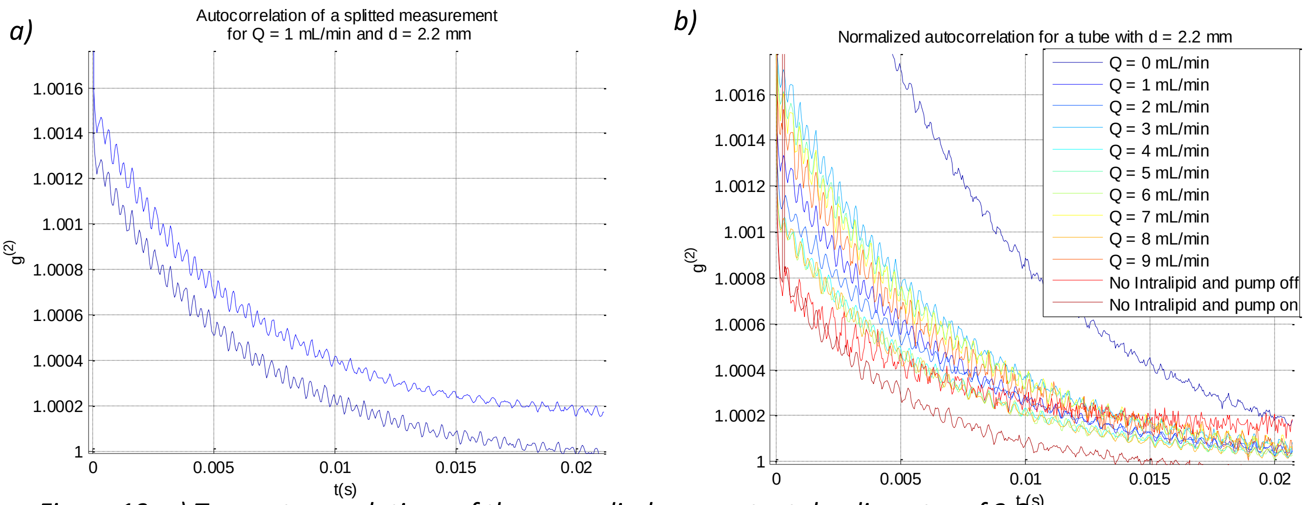

Figure 19. a) Two autocorrelations of the same discharges at a tube diameter of 3.2 mm
b) Autocorrelations of different discharges at a tube diameter of 3.2 mm.

The same is done for the measurement with Q = 1 mL/min and d = 3.2 mm, which can be seen in Fig. 20. If we compare Fig. 20a to Fig. 20b the autocorrelation for Q = 1 mL/min can overlap the first three lowest discharges. At the other hand the Fig. 19a and Fig. 20a. are less accurate, because it used half of the frames compared to figures 19b and 20b.

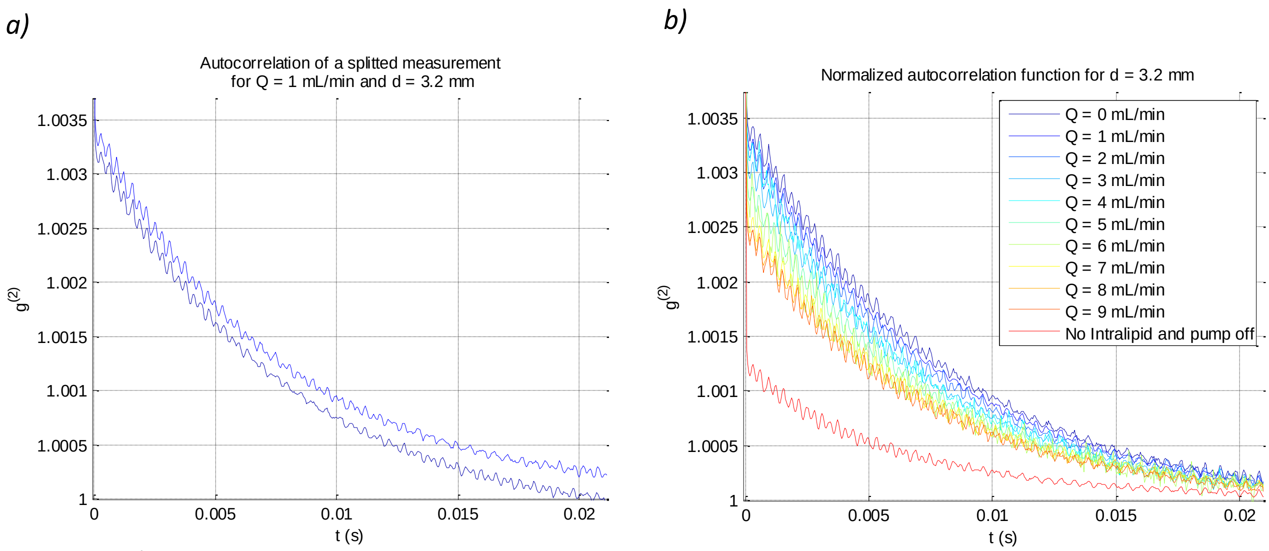

Figure 20. a) Two autocorrelations of the same discharges at a tube diameter of 3.2 mm
b) Autocorrelations of different discharges at a tube diameter of 3.2 mm.

3.4.2 Comparison to theory

As seen in section 3.1.1 the LDF model has decorrelation times in the range of 10^{-8} seconds. This is much less than the sample and shutter time in the measurement. Therefore it can not be compared. For de DWS model the ranges of the decorrelation time are in that of the measurement. One problem is that the experimental factor β is unknown because of the unknown contribution of noise to the peak height. In Fig. 21 a β is chosen, so that the beginning of the autocorrelation looks familiar.

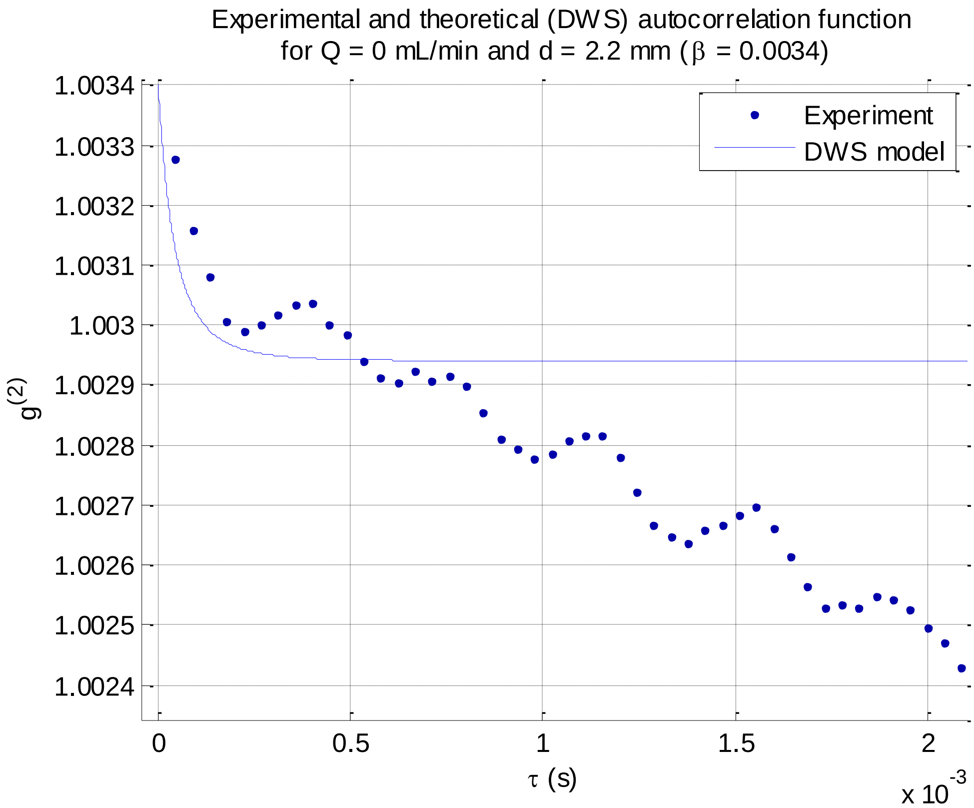

Figure 21. The autocorrelation of the Experimental compared with the theoretical (DWS model) one for Q = 0 mL/min and d = 2.2 mm

In Fig. 21 it can be seen that theoretical autocorrelation still decorrelates much faster than the experimental one. Also, if a value of β is used that gives reasonable agreement in the offset, the level to which the theoretical function eventually decorrelates is far from that of the experimental one.

In Fig. 21 the ratio I_0/I_{sc} is the theoretical ratio is used. To obtain a better fit to the offset and end level of the experimentally found curve, this ratio was changed. In Fig. 22 the situation for $I_0 = I_{sc}$ can be seen; the starting and end points agree in this case, but the theoretical curve decreases much faster than the experimental one. This fast decrease originates from *G(τ)* the fast decrease of G(τ).

For the measurement with d = 3.2 mm the graphs will look similar.

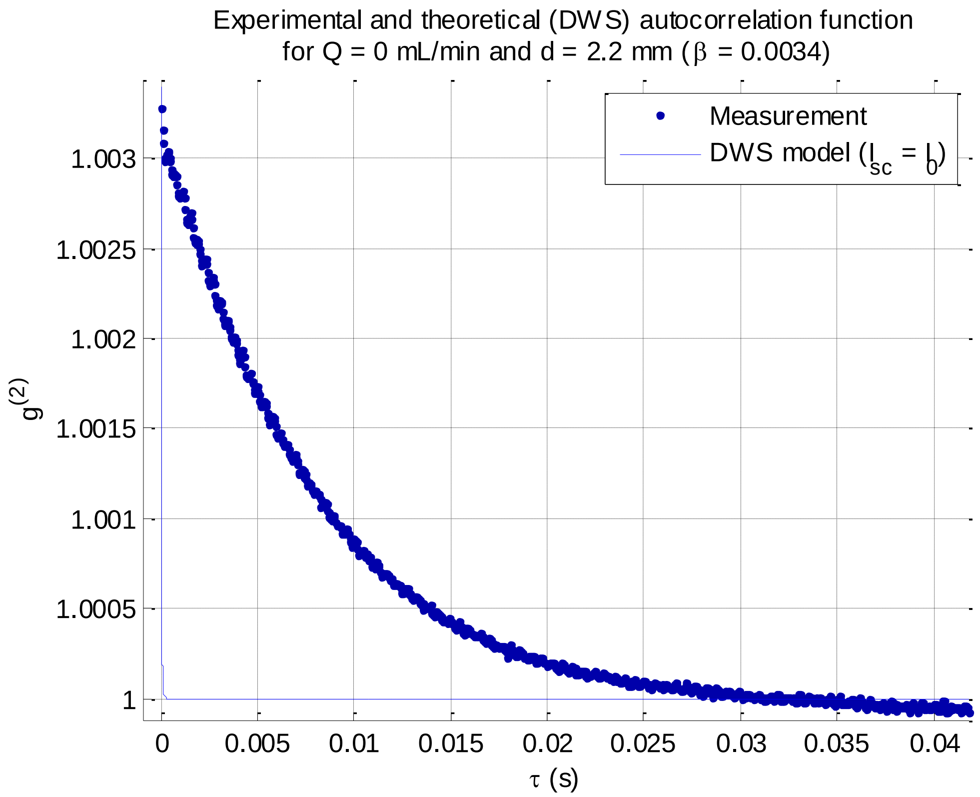

Figure 22. The autocorrelation of the Experimental compared with the theoretical (DWS model) one. Here the ratio I_{sc} / I_0 is changed for Q = 0 mL/min and d = 2.2 mm

3.5 Discussion

In the measurements a difference can be seen in the speckle decorrelation of a tube with stationary Intralipid and with Intralipid flowing through. There can be concluded that for a discharge of zero, the decoration originating from the Brownian motion of the Intralipid beads can be seen.

For the measurement for d = 2.2 mm and without Intralipid it can be seen that the decorrelation is almost the same as with flowing Intralipid. This can be explained by the fact that with no Intralipid present there is an almost stable sample, which gives less decorrelation. When the Intralipid enters the tube the contrast decreases from around 0.24 to 0.15. This can also be seen by the blurring of the measured frames. By this blurring the decorrelation will also be less. Still it can be seen that for a discharge of zero the autocorrelation starts higher. Therefore it is likely that the decorrelation, caused by the translation movement of Intralipid takes place in time scales shorter than the shutter time of the camera, while the effects of Brownian motion take place at the edge of (but within) the detection limit.

In the measurement for d = 3.2 mm the effect of different discharges can be seen. Because the cross sectional area of the tube is larger in this case, more light will pass through the tube. Therefore there will be more decorrelation than in the case of d = 2.2 mm. That the total decorrelation decreases with increasing discharges can be caused by part of the decorrelation still taking place in a timescales shorter than the time between two frames, causing the second data point of a higher discharge to become lower than that of lower discharge.

It can also be seen that the autocorrelation with no Intralipid starts higher for d = 3.2 mm than for d = 2.2 mm. This is strange, because it is expected that if there is a bigger empty tube the sample will be more stable. We have not found a satisfying explanation for this fact.

There is an influence of the pump: if the pump is on the speckle pattern decorrelate more. This can be explained by the vibration of the tube due to motor of the pump. However, this effect is small compared to the amount of decorrelation of the sample itself. It needs to be studied where the 3750 Hz in our measurements is coming from, this does not come from the pump, because it is also present when the pump is off.

To find out how much the autocorrelation function could differ from measurement to measurement, we split up one measurement in two and compared the autocorrelation functions. The disadvantage of this method is that only half of the data is used, while accuracy will increase if you use more data. In future experiments it can be worthwhile to measure one discharge more times for the same tube. It could also be interesting to see how the autocorrelation function will look at bigger sizes of the tube.

It must be noted that the absorption and the scattering coefficient of Intralipid gives an approximation of the real values, because the content of Intralipid is dependent on the factory where it is made. Therefore the values in literature are deviating from each other. So it is better to measure these coefficients first for other measurements.

If the theoretical models and the measurements are compared, it can be concluded that they are not the same. The LDF model gives a decorrelation time scale in the order of 10^{-8} s, which is much less than can be measured in our setup. The DWS model gives a time scale in the order 10^{-5} s, which is closer to our measurement.

After all it is most likely that the decorrelation because of the translation of the Intralipid happens in time scales shorter than the time between two camera frames, ending up in the peak of the measured autocorrelation. This also can explain why the autocorrelation function for d = 3.2 decorrelates less when the discharge increases. However, in the peak of the autocorrelation there can also be a lot of noise. It would be good to investigate how this noise can be removed as much as possible; a complicating factor is that the camera used did not have a bias voltage, giving a non-gaussian distribution of readout noise. Because the shutter time is very small, there will also be a lot of shot noise. This makes that information of the decorrelation in the first points of the autocorrelation function remains hidden.

In the measurements the contrast value is low, an empty tube gives a contrast value of 0.24 and with Intralipid it decreases to around 0.16. For further research there can be considered to get a higher contrast value, this can be done by increasing the power of the beam, or changing the speckle size on the camera. A camera with still lower shutter times and higher frame rates might give improvement, and give insight in processes happening faster than could be measured in this research. This might give more clues about the validity of both the LDF and DWS models.

4. Conclusions

In this report, the influence of a tube with scattering fluid inside a stable tissue phantom on decorrelation of transmitted laser speckle was investigated. As a first approximation of the amount of light passing through the tube, the following relation was derived:

$$\frac{P_{trans,tube}}{P_{trans}} = \frac{4r_t}{\pi r}\left(\frac{z_e + z_t}{L + 2z_e}\right) \tag{39}$$

Based on this result, an equation was derived for the normalized autocorrelation function of the speckle intensity, given by:

$$g_\beta^{(2)}(\tau) = 1 + \beta\left(\left(1 - \frac{2r_t}{\pi r}\right)^2 + 2\left(1 - \frac{2r_t}{r}\right)\frac{2r_t}{r}|G(\tau)| + \left(\frac{2r_t}{r}\right)^2 |G(\tau)|^2\right) \tag{51}$$

The intermediate scattering function $G(\tau)$ was found from two different models, one used in Laser Doppler Flowmetry, the other in Diffusing Wave Spectroscopy. An interesting paradox between these models was discussed: wavelength dependence, which is present in the latter, is absent in the first. The so called Bonner-Nossal approximation, done in the derivation of the LDF model, was found to be the cause of this difference. To our insights, this approximation is not fully supported by argument.

Based on the different models, predictions were made about the decorrelation time scales of the speckle intensity. These were in the order of 10^{-8} s for the LDF and 10^{-5} s for the DWS model.

With some elementary fluid dynamics, an expression was found for the upper limit of decorrelation times:

$$t_{95} = \frac{\lambda \pi r_t^2}{0.2\,Q}. \tag{81}$$

This expression gives time scales of 10^{-5} to 10^{-4} s for a tube of 2.2 mm diameter, and 10^{-4} to 10^{-3} s for a tube of 3.2 mm diameter, for discharges in the range of 1 to 9 mL/min.

The experiments indicate that speckle decorrelation caused by Brownian motion takes place in time scales of 10^{-4} to 10^{-2} s. On the other hand, effects from translational motion most likely take place in time scales barely detectable (for d = 3.2 mm) or not detectable at all (for d = 2.2 mm) with our setup. Better ways of normalizing, taking into account the noise level, could bring more clarity, since then information about β can also be extracted from the first data point. When noise can be accounted for, it becomes more clear what the actual time scales of decorrelation of the sample with fluid are (apart from the noise). Furthermore, investigation of contrast values (LASCA) could bring an interesting approach to analyzing the speckle, since then the frame rate and shutter time of the camera are less likely to be a limiting factor.

The experimentally found autocorrelation functions are very different from the theoretical ones. Though the shape resembles the DWS curves, the time scales of the experimentally seen effects are much lower than the ones predicted by theory. Fitting the curves appears impossible: for the theoretically predicted I_0/I_{sc}, there is no value of β that gives a good agreement with both offset and end level of the curves. This can only be achieved by setting $I_{sc} = I_0$, but even then, the time scales differ at least a factor 100.

Though the DWS model seems to be the most promising candidate for describing the decorrelation of speckle, work needs to be done to adjust this model to the given situation. A discussion of possible improvements of the theoretical models was given at the end of chapter 2, in section 2.5.

The time scale at which speckle decorrelation from Intralipid in a mm-sized tube inside a Delrin slab happens, is likely to be in the order of 10^{-2} to 10^{-5} s, or even faster for high translational velocities. With current SLM devices it is just possible to adjust the wavefront in a time scale of 10^{-4} s. Noting that actual blood flow rates can be even higher than the flow rates used in this research, it remains an open question whether, with an optimized wavefront shaping setup, imaging inside in-vivo tissue might be possible in the future.

To conclude and summarize, further research is recommended in three areas:

- Improving the theoretical model and further investigating the applicability and limits of the LDF and DWS (and possibly other) models;
- Performing experiments that can give more conclusive results on decorrelation time scales and the shape of the actual autocorrelation function, incorporating any possible noise effects (shot noise, readout noise) as much as possible;
- Moving towards a setup more closely resembling actual human tissue (for instance by including microcapilary or using softer materials than Delrin), in the end working towards clinical application.

In the end, it remains an interesting question whether it is needed to adjust wavefront shaping devices to be able to keep up with the changes of the transmission matrix caused by (fast-moving) dynamical elements, or that it is possible to find a way around this. It is not unthinkable that the more stable parts of some tissues can cause enough relatively stable speckle, enabling wavefront shaping to be done while totally disregarding the fastest dynamic elements (like blood vessels). By expanding our relatively simple diffusion model by using more realistic three-dimensional perfusion and incorporating the return probability of light to dynamic elements, it might be possible to shine more light upon this puzzle. Until then, the answer to this question is still waiting to be uncovered.

References

[1] J. F. de Boer, *optical fluctuations on the transmission and reflection of mesoscopic systems*, PhD thesis, University of Amsterdam (1995)

[2] D.A. Boas, *Diffusive photon probes of structural and dynamical properties of turbid media: theory and biomedical applications*, chapter 4, PhD thesis, University of Pennsylvania (1996)

[3] R.F. Bonner and R. Nossal, *Model for laser Doppler measurements of blood flow in tissue*, Appl. Opt. **20** pp. 2097-2107 (1981)

[4] T. Binzoni, T.S. Leung, M.L. Seghier and D.T. Delpy, *Translational and Brownian motion in laser-Doppler flowmetry of large tissue volumes*, Phys. Med. Biol. **49** pp. 5445-5458 (2004)

[5] T. Binzoni, T.S. Leung, D. Rüfenacht and D.T. Delpy, *Absorption and scattering coefficient dependence of laser-Doppler flowmetry models for large tissue volumes*, Phys. Med. Biol. **51** pp. 311-333 (2006)

[6] C.M. Sorensen, R.C. Mockler and W.J. O'Sullivan, *Depolarized correlation function of light double scattered from a system of Brownian particles*, Phys. Rev. A **14** pp. 1520-1532 (1976)

[7] T. Li and M.G. Raizen, *Brownian Motion at short time scales*, Ann. Phys. (Berlin) **525** (4) pp. 1-15 (2013)

[8] R. Zwanzig and M. Bixon, *Compressibility effects in the hydrodynamic theory of Brownian motion*, J. Fluid Mech. **69** (1) pp. 21-25 (1975)

[9] D.J. Pine, D.A. Weitz, P.M. Chaikin and E. Herbolzheimer, *Features of Diffusing Wave Spectroscopy*, in J. Abiss and A.E. Smart, editors, *OSA Proceedings on Photon Correlation Techniques and Applications*, volume 1 pp. 35-43, Optical Society of America, Washington, DC (1988)

[10] I. Fredriksson, C. Fors and J. Johansson, *Laser Doppler Flowmetry - a Theoretical Framework*, Department of Biomedical Engineering, Linköping University (2007), www.imt.liu.se/bit/ldf/ldfmain.html

[11] M. Sundberg, T. Lindbergh and T. Strömberg, *Monte Carlo simulations for estimation of backscattered light intensity using an optical source-detector fibre array probe on convex Delrin pieces*, http://www.biop.dk/biophotonics05/posters/sundberg_poster.pdf/

[12] S. Jacques, *Optical properties of "Intralipid™", an aqueous suspension of lipid droplets.* Oregon Medical Laser Center, 1 April 1998, http://omlc.ogi.edu/spectra/intralipid/

[13] A. Giusto, R. Saija, M.A. Iatì, P. Denti, F. Borghese and O. I. Sindoni, *Optical properties of high-density dispersions of particles: application to intralipid solutions*, App. Opt. **42** (21) pp. 4375-4380 (2003)

[14] R. Michels, F. Foschum and A. Kienle, *Optical properties of fat emulsions*, Optics Express **16** (8) pp. 5907-5925 (2008)

[15] P. N. den Outer and Th. M. Nieuwenhuizen, *Location of objects in multiply scattering media*, J. Opt. Soc. Am. A **10** (6) pp. 1209-1218 (1993)

[16] S. Feng and F. Zeng, *Monte Carlo Simulations of Photon Migration Path Distributions in Mutiple Scattering Media*, SPIE Vol. 1888 pp. 78-89 (1993)

[17] S. Del Bianco, F. Martelli and G. Zaccanti, *Penetration depth of light re-emitted by a diffusive medium: theoretical and experimental investigation*, Phys. Med. Biol. **47** pp. 4131-4144 (2002)

[18] S. Feng, F.A. Zeng and B. Chance, *Photon migration in the presence of a single defect: a perturbation analysis*, App. Opt. **34** (19) pp. 3826-3837 (1995)

[19] A.B. Konovalov, V.V. Vlasov, A.G. Kalintsev, O.V. Kravtsenyuk and V.V. Lyubimov, *Time-domain diffuse optical tomography using analytic statistical characteristics of photon trajectories*, Quantum Electronics **36** (11) pp. 1048-1055 (2006)

[20] H. Cheng, Y. Yan and T. Q. Duong, *Temporal statistical analysis of laser speckle images and its application to retinal blood-flow imaging*, Optics Express **16** (14) pp. 10214-10219 (2008)

[21] P. Zakharov, A.C. Völker, F. Buck, B. Weber and F. Scheffold, *Non-ergodicity correction in laser speckle biomedical imaging*

[22] C. Hanotin, P. Marchal, L. J. Michot, C. Baravian and S. K. de Richter, *Dynamics of vibrated granular suspensions probed by mechanical spectroscopy and diffusing wave spectroscopy measurements*, Soft Matter, 2013, **9**, p. 9352

[23] J.X. Zhu, D.J. Pine and D.A. Weitz, *Internal reflection of diffusive light in random media*, Phys. Rev. A **44** (6) pp. 3948-3959 (1991)

[24] P. Zakharov, F. Cardinaux, and F. Scheffold, *Multispeckle diffusing-wave spectroscopy with a single-mode detection scheme*, Phys. Rev. E **73** 011413 (2006)

[25] P. Snabre and J. Crassous, *Multispeckle diffusing wave spectroscopy of colloidal particles suspended in a random packing of glass spheres*, Eur. Phys. J. E **29** pp. 149–155 (2009)

[26] A. Humeau, W. Steenbergen, H. Nilsson and T. Strömberg, *Laser Doppler perfusion monitoring and imaging: novel approaches*, Med. Bio. Eng. Comput. **45** pp. 421-435 (2007)

[27] H. J. van Staveren, C.J.M. Moes, J. van Marie, S.A. Prahl and M. J.C. van Gemert, *Light scattering in Intralipid-10% in the wavelength range of 400-1100 nm*, App. Opt. **30** (31) pp. 4507-4514 (1991)

[28] D. Irwin, *Influence of tissue absorption and scattering on diffuse correlation spectroscopy blood flow measurements*, Master Thesis, University of Kentucky, paper 136 , http://uknowledge.uky.edu/gradschool_theses/136 (2011)

[29] R. Berg, S. Andersson-Engels, O. Jarlman, and S. Svanberg ; *Time-gated viewing studies on tissue like phantoms*; App. Opt. **35**,(19) (1996)

[30] Biju Cletus, Paul Martinsen, Vincent Andrew McGlone and Rainer Künnemeyer, *Temperature-dependent optical properties of Intralipid® measured with frequency-domain photonmigration spectroscopy*, Journal of Biomedical Optics 15, January/February 2010

[31] C. Mobley; *Light and Radiometry;* Geometry Open Optics webbook; http://www.oceanopticsbook.info/view/light_and_radiometry/geometry (2010)

[32] P. Nelson; *Biological Physcis: Energy, Information, Life;* (2002)

[33] A.P. Mosk, A. Lagendijk, G. Lerosey and M. Fink; Controling waves in space and time for imaging and focusing in complex media; Nature photonics, 2 May 2012

[34] B.R. Munson, D.F. Young, T.H. Okiishi and W.W. Huebsch; *Fundamentals of Fluid Mechanics*, 6th edition; John Wiley & Sons (Asia) Pte Ltd (2010)